UNIVERSIDAD DE CHILE
FACULTAD DE CIENCIAS FÍSICAS Y MATEMÁTICAS
DEPARTAMENTO DE INGENIERÍA CIVIL

MODELING HEAT TRANSFER IN SEVERELY CONFINED ENVIRONMENTS

TESIS PARA OPTAR AL GRADO DE MAGÍSTER EN CIENCIAS DE LA INGENIERÍA, MENCIÓN RECURSOS Y MEDIO AMBIENTE HÍDRICO

MEMORIA PARA OPTAR AL TÍTULO DE INGENIERO CIVIL

PABLO IGNACIO VERGARA COLMANN

PROFESOR GUÍA:
JUVENAL LETELIER VILLALÓN

MIEMBROS DE LA COMISIÓN:
HUGO ULLOA SÁNCHEZ
YARKO NIÑO CAMPOS

SANTIAGO DE CHILE
2023

MODELADO DE TRANSFERENCIA DE CALOR EN ENTORNOS SEVERAMENTE CONFINADOS

La energía geotérmica se posiciona como una solución sostenible a las fuentes de energía tradicionales. Gran parte de los reservorios geotermales que se aprovechan son sistemas dominados por el transporte advectivo de calor. Una celda de Hele Shaw puede servir para el estudio a escala de laboratorio de lo que ocurre en un medio poroso, en donde la separación entre placas tiene una relación directamente proporcional al coeficiente de permeabilidad K de un medio poroso. Un estudio reciente utilizando un modelo en celdas de Hele Shaw (HSM) (Letelier, Mujica, & Ortega, 2019) ha demostrado que la relación entre la separación de las placas y la altura es importante a la hora de estudiar el comportamiento del sistema, diferenciándose de los resultados obtenidos utilizando un modelo completamente darciniano. Esto indica que en medios con un coeficiente de permeabilidad K importante, como podría ser una falla geológica, los flujos no estarían bien representados solamente con la ley de Darcy.

La motivación de este estudio se centra en el desafío de inyectar un fluido frío en reservorios geotermales, una práctica común para el mantenimiento de la presión y el volumen en tales reservorios. Esta inyección podría alterar las propiedades termodinámicas del reservorio, potencialmente conduciendo a disminuciones de temperatura o incluso a situaciones extremas de apagón geotérmico. Debido a que el fluido frío es más denso, tiende a descender y mezclarse con las capas límite del sistema. Sin embargo, antes de abordar este problema, es crucial comprender la dinámica de estas capas límite. Los objetivos de este estudio son dobles: i) validar el modelo HSM mediante la comparación con estudios previos en la literatura, y ii) caracterizar capa límite térmica a partir de los números adimensionales que dominan el problema.

El estudio utiliza el modelo de transporte de calor en celdas Hele-Shaw (Letelier et al., 2019), que representa una falla geológica vertical a escala de laboratorio o un medio permeable en aproximación cuasi-2D. El transporte de calor se examina en términos de parámetros adimensionales: el número de Rayleigh (Ra), que caracteriza el régimen de transporte (convectivo o conductivo), el número de Prandtl (Pr), que representa la relación entre la difusividad del momento y la difusividad térmica, y la anisotropía de la celda (ϵ), la relación entre la apertura de la celda y la altura. La respuesta térmica del sistema se estudia mediante el cálculo del número de Nusselt (Nu), que caracteriza el transporte de calor en un sistema y corresponde a la relación entre la transferencia de calor por convección y por conducción en la frontera del fluido.

Los principales hallazgos de este estudio son que i) El modelo logra reproducir resultados fielmente hasta $\epsilon^2 Ra = 0.06$ (preliminarmente), y ii) para regímenes de alto Prandtl ($Pr > 1$) el transporte de calor no se afectado por cambios en este número, y que el número de Prandtl se vuelve significativo para $Pr < 1$. La investigación aporta conocimientos valiosos sobre el comportamiento de la convección térmica en geometrías confinadas y sus implicaciones para la ingeniería de reservorios geotermales y la modelación de acuíferos.

MODELING HEAT TRANSFER IN SEVERELY CONFINED ENVIRONMENTS

Geothermal energy is emerging as a sustainable solution to traditional energy sources. Thanks to technological advancements, it is now economically viable to extract energy from the subsurface in previously inaccessible locations. A significant portion of exploited geothermal reservoirs are systems dominated by advective heat transport, and some of them feature geological structural controls such as faults and/or fractures. A Hele-Shaw cell can be utilized for the laboratory-scale study of phenomena occurring within porous or permeable media, where the plate separation directly correlates with the permeability coefficient K of the medium. Recent research using the Hele-Shaw model (HSM) introduced by Letelier et al. (2019) has shown that the aspect ratio of the cell, the ratio between plate separation and height, plays a crucial role in the system's dynamics. This finding differs from results obtained using a fully Darcian model, indicating that in highly permeable media, such as geological faults, flows cannot be adequately represented solely by Darcy's law.

The motivation behind this study lies in the challenge of injecting a cold fluid into geothermal reservoirs, a common practice for maintaining pressure and volume in such reservoirs. This injection could alter the thermodynamic properties of the reservoir, potentially leading to temperature decreases or even extreme geothermal shutdown situations. As the cold fluid is denser, it tends to descend and mix with the boundary layers of the system. However, before addressing this issue, it is crucial to understand the dynamics of these boundary layers. The objectives of this study are twofold: i) to validate the HSM model by comparing it with previous studies in the literature, and ii) to characterize the thermal boundary layer based on the dimensionless numbers that govern the problem.

The study utilizes the heat transport model for a Hele-Shaw cell (Letelier et al., 2019), which represents a vertical geological fault at a laboratory scale or a quasi-2D permeable medium. Heat transport is examined in terms of dimensionless parameters: Rayleigh number (Ra), characterizing the transport regime (convective or conductive), Prandtl number (Pr), representing the ratio between momentum and thermal diffusivity, and the anisotropy of the cell (ϵ), the ratio between cell aperture and height. The thermal response of the system is studied by calculating the Nusselt number (Nu), which characterizes heat transport in a system and corresponds to the ratio of convective to conductive heat transfer at the fluid boundary.

The main findings of this study are that i) The model exhibits results that align with expectations up until $\epsilon^2 Ra = 0.06$ (preliminarily), and ii) for high Prandtl regimes ($Pr > 1$), the Prandtl number does not affect the total heat transport in the cell, but it becomes significant for $Pr < 1$. The research contributes valuable insights into the behavior of thermal convection in confined geometries and its implications for geothermal reservoir engineering and aquifer modeling.

Order and simplification are the first steps toward the mastery of a subject.

Thomas Mann

Agradecimientos

Quiero comenzar expresando mi profundo agradecimiento a mis padres, Sergio y Cecilia. Gracias por ofrecer un apoyo incondicional a lo largo de mi vida. Mis logros son y siempre serán el fruto de su inquebrantable esfuerzo y dedicación. Les estoy muy agradecido por todo.

A mi hermana Daniela, quien ha sido mi compañera de viaje a lo largo de todos estos años y ha demostrado ser un pilar fundamental en mi vida.

Un reconocimiento especial a mis abuelos, Eduardo y Adriana, cuya presencia constante ha sido esencial para mí. Siempre han estado allí, brindando su amor y apoyo incondicional.

A mis tíos y primos, Eduardo, Paula, Josefa, Matías, Pía y Montse, les agradezco por estar siempre a mi lado y ser parte de esta familia tan unida.

Montse, agradezco sinceramente por formar parte de mi vida en este último año y por mostrarme una perspectiva del mundo que desconocía.

A mi Profesor Guía, Juvenal Letelier, le agradezco por presentarme este desafiante problema y por su disposición constante para guiarme y orientar mi trabajo. A Hugo Ulloa, gracias por recibirme en Estados Unidos y por ser parte integral de esta experiencia única.

A mis amigos, Carlos, Diego, Felipe, Benjamín, Agustín, Ignacio y Fernando, les agradezco por acompañarme durante mi tiempo en la universidad. Los momentos compartidos y los recuerdos perdurarán en mi memoria.

Un agradecimiento especial a mis amigos de la salita: Felipe, Naro, Gabi, Kari, Fabián y Alexis. Gracias por las risas, los almuerzos, los días de juegos de mesa y los after office. Gracias Jacque por tener siempre la mejor dispocisión para ayudarme en cualquier cosa.

Table of Content

List of Figures

Chapter 1

Introduction

1.1. Introduction and motivation

1.1.1. Geothermal energy

Geothermal energy is generated from the internal heat produced by the earth (Barbier, 2002) and stored in places called geothermal reservoirs. It is positioned as a novel alternative to traditional energy sources, such as natural gas, oil, and coal (K. Li et al., 2015). In recent times, many countries are aiming to transition from a fossil fuel-dependent electricity generation system to a sustainable one that relies on renewable resources. This shift is driven by ongoing political discussions surrounding carbon dioxide emissions targets, global warming limits set by the UN, and energy policy considerations (Christensen & Hain, 2017).

Geothermal energy offers several advantages in this regard, including low greenhouse gas emissions, contributions to sustainable development, diversification of energy resources, and improvements to existing energy systems (Christensen & Hain, 2017). It is noteworthy that geothermal energy provides distinct advantages compared to other renewable sources like solar or wind power. For instance, geothermal energy offers a stable production profile and consistently high capacity factors exceeding 90% in many cases. Furthermore, geothermal energy has a minimal ecological impact due to its independence from weather conditions and its efficient use of space (K. Li et al., 2015).

The definition of a geothermal system has evolved over time. Initially, only the heat transported by the circulation of steam or hot water close enough to the surface was taken into account, i.e. only the heat transported by convection. However, it is now known that heat is present in enormous and practically inexhaustible quantities in the earth's crust, but generally at depths too great to be exploited industrially (Barbier, 2002). Nowadays, thanks to technological advances, the concept of enhanced or *engineered geothermal systems* (EGS), which refer to technological reservoirs in which stored thermal energy can be extracted from the subsurface even in areas of low or moderate thermal flux. This can be done, for example, by injecting fluids or generating fractures, making it economically feasible to extract heat from the subsurface. EGS has significantly increased the global geothermal potential, and has evolved the definition of a geothermal system to any localized geological environment where portions of the Earth's thermal energy can be extracted from natural or artificially induced circulating fluids and transported to a point of use (Moeck, 2014).

The geological conditions in which the geothermal system is immersed such as lithology, faults, fractures, stress field, diagenesis, geomechanics, geochemistry and fluid chemistry control key parameters like high porosity/permeability zones, flow directions, temperature distribution and overall system behavior during injection and production, which ultimately determine whether geothermal fluids have the ability to migrate to shallower crustal levels (Moeck, 2014). High heat fluxes through the earth's crust generate surface manifestations like hot springs, fumaroles, and mud pools. These manifestations provide valuable information about the underlying flow paths and geological structures (Olvera-García et al., 2020). In fault- or fracture-controlled geothermal systems, where convective heat transport dominates, there is evidence of rapid fluid migration along these preferential flow pathways (Pruess & Bodvarsson, 1984).

1.1.2. Geothermal resources in Chile

Chile is considered as one of the most important geothermal provinces in the world. Most of the thermal zones are located along the Andes Mountains, and are associated with the volcanism of the Quaternary period. The volcanic-geothermal activity is mainly controlled by the subduction processes of the Nazca and Antarctic oceanic plates under the South American continental plate (Lahsen, 1988).

Geothermal resources in Chile remain largely untapped, presenting a significant opportunity as a clean source for electricity generation. Currently, the country heavily relies on imported fossil fuels for nearly 85% of its electricity production and over 75% of its overall energy consumption. The Northern Chile geothermal zone boasts approximately 90 identified areas with hot springs, indicating the potential for geothermal development. Notable progress in exploration has been made in the Colpitas, Apacheta, Pampa Lirima, and El Tatio-La Torta geothermal prospects, representing the most advanced programs in the region (Lahsen et al., 2015). Exploiting these geothermal resources could contribute to reducing Chile's dependence on fossil fuels while simultaneously fostering a cleaner and more sustainable energy sector.

A notable example of the use of geothermal energy in Chile is the Cerro Pabellón plant (Figure 1.1), which is located on the high plateau of the Atacama Desert in the Antofagasta Region. It is the only operational geothermal power plant in South America and the highest of its kind in the world, as it is located 4.500 meters above sea level. In 2022, its third 33 MW generating unit came into operation, which added to the 48 MW of the two units already in operation, gives Cerro Pabellón a total power of 81 MW and a total production of 600 GWh per year, avoiding the emission of 470,000 tons of CO2 into the atmosphere [1].

Another example of a large geothermal field recently studied is El Tatio, located in northern Chile on the western flank of the Andes, which is a system of geysers, hot springs, mud pools and shallow hot springs, and may be a multiple reservoir, following a fault-controlled convective system model (Letelier et al., 2021).

[1] Data from enel.cl

Figure 1.1: Panoramic view of Cerro pabellón geothermal power plant in Chile. Figure from Enel.cl

1.1.3. Reinjection in geothermal fields

Prior to the 1980s, geothermal reservoirs were not managed efficiently, as extracted water was often discharged into surface water bodies, leading to environmental risks and lower energy recovery rates. In the 1980s, reinjection of wastewater into geothermal reservoirs was introduced as an effective solution to this problem (Kamila et al., 2021). Wastewater reinjection also serves other purposes, such as maintaining system pressure, preventing intrusion of fluids from other aquifers, and sustaining geothermal exploitation by providing necessary recharge to maintain fluid volume conditions in the reservoir (Shortall, Davidsdottir, & Axelsson, 2015).

Although geothermal energy is classified as renewable, its sustainability is not unconditional and can be compromised by several factors. For instance, injecting cooler water into the reservoir can cause a phenomenon called *geothermal breakthrough*, in which the thermal and pressure conditions of the system are altered due to the injection of cold fluids (Bödvarsson & Tsang, 1982). This problem has been observed in several geothermal plants around the world (Kamila et al., 2021). Numerical models have been developed to characterize the dynamics of reinjection (Blöcher et al., 2010; Saeid et al., 2013; T. Li et al., 2016; H. Liu et al., 2020), which provide information about the temperature drop of geothermal fluids over time and different thermal dynamics. However, these simulations are not direct numerical simulations.

There are many questions regarding fluid reinjection that can be investigated. For example, how the system respond to variations in the injection temperature, the vertical position of the cold fluid injection, the distance between the reinjection well and the injection well, determine the time it takes for a system to return to its natural state after a finite duration (t_{iny}) of cold fluid injection, among others. *While this problem constitutes the central motivation of this study, it is imperative to first comprehend the physics governing it, understand its response to variations in fundamental physical parameters, and gain a more precise char-*

acterization of the fluid dynamics occurring under conditions without the injection of cold water.

1.1.4. Representation of the problem and heat transfer

The study of the dynamics of geothermal reservoirs and what happens inside them is a complex matter. First of all, porous media are opaque media, i.e. we cannot visualize the processes that are occurring. In addition, most of these types of reservoirs have length and depth scales of the order of meters, even kilometers. The time scales on which subsurface processes occur are also high, on the order of days, even years or more. The geometries of the aquifers are also complicated and far from ideal. Hence, studying geothermal reservoirs is a challenge and a difficult problem to address.

A Hele-Shaw cell is a device commonly used in laboratory experiments to simulate the fluid flow through a porous medium. It consists of two parallel flat plates separated by a small gap, filled with a fluid (Nield & Bejan, 2012). The cell allows for direct visualization of the fluid flow patterns, making it easier to study the influence of various factors, such as fluid properties, pressure gradients, and geometrical features, on the flow behavior. The separation between plates is directly related to the porosity in a porous medium (Saffman, 1986). Therefore, it is a useful tool for the study of flow in porous media.

The dynamics of heat transfer in the subsurface can be represented by the classic Rayleigh Bénard fluid mechanics problem (RBC), which consists of a fluid confined between two parallel plates at constant temperature, such that the temperature of the lower plate T_{bot} is greater than the temperature of the upper plate T_{top}. Due to buoyancy effects, when the temperature difference between the plates exceeds a critical value T_{crit}, the conductive motionless state is unstable and convection occurs (Bodenschatz et al., 2000).

In classical free fluids RBC, there are 2 dimensionless numbers that dominate the problem (Ahlers, Grossmann, & Lohse, 2009). First is the Rayleigh number Ra, which characterizes the transport regime (convective or conductive) and is defined as the ratio between buoyant and diffusive effects (all the mathematical formulation can be found in Chapter 2). The second is the Prandtl number Pr which is the ratio of momentum diffusivity to thermal diffusivity. This parameter measures the relative importance of the nonlinear terms in the equations of motion. Also has a direct relationship with the boundary layers of the system, since boundary layers are environments where conductive transport dominates. The system response is mainly measured by the Nusselt number Nu, which is the ratio of convective to conductive heat transfer at a fluid boundary.

RBC has also been studied in Hele Shaw cells. Letelier et al. (2019) demonstrated that the separation between the cell plates affects the thermal response of the system. They used a model that incorporates inertial corrections to Darcy's law and the phenomenon of hydrodynamic dispersion. *The limits of this Hele Shaw cell model (HSM) are not yet clear.* As mentioned above, the separation of the plates in a Hele Shaw cell is directly related to the permeability in a porous medium, therefore, the heat transfer dynamics may be affected, for example, in a highly fractured medium with a high permeability coefficient.

In RBC, the thermal boundary layer plays a key role in determining heat transfer (Ahlers et al., 2009; King et al., 2013; Ulloa & Letelier, 2022). In porous media, Otero et al. (2004) studied a model in 2D, found that for values of $Ra \geq 4\pi^2$ the system is unstable and large-scale convective cells appear that enhance heat transport and that from $Ra > 1200$, instead of convective cells, the formation of thermal plumes predominates. They also observed a phenomenon of clustering of hot (or cold) mass in the boundary layer up to a certain break point where the rise of the plumes begins. Hewitt, Neufeld, and Lister (2012) also in a 2D porous medium model, for high Rayleigh regimes ($Ra \geq 1300$) recognizes three zones of importance: The inner region, dominated by a predominantly vertical heat transport in mega-plumes or columns whose wavelength is quite regular and Ra-dependent; The upper and lower part of the domain where there are thin diffusive boundary layers, in which there are intermittent short wavelength instabilities that drive the growth of proto-plumes; and finally between the boundary layer and the inner region is a region where the dynamics are characterized by rapid protoplume growth and mixing. Studying fluid mixing in Hele-Shaw cells, Ulloa and Letelier (2022) conclude that megaplumes detach from the thermal boundary layer and occupy most of the domain, creating preferential pathways to transport fluid from top to bottom, homogenizing the temperature of the inner region and thus, increasing the degree of mixing of the system. They also observed that the megaplumes have an impact on the thermal boundary layers, reducing their size and forcing the emerging protoplumes to diverge laterally and merge with the megaplumes. Furthermore, the authors propose a method to quantify the degree of mixing in the system based on the height of the thermal boundary layer. They suggest an expression to calculate the boundary layer height; however, it is important to note that all numerical simulations and results presented in the study are based on a Prandtl number (Pr) value of 7.

It is essential to understand how the system behaves under variations of the Prandtl number before addressing the reinjection problem. Because the injected fluid will have a lower temperature than the ambient fluid and, consequently, the injected fluid will tend to sink to the bottom of the domain and mix with the geothermal fluid. This mixing will affect the dynamics of the boundary layer, which is closely related to the Prandtl number.

1.1.5. Contributions of this work

Based on the above, the questions to be solved are:

1. To what extent can the HSM retain the physics of 3D convection in confined environments?

2. What is the effect of the Prandtl number on the heat transport dynamics in Hele Shaw cells?

The main objectives of this study is to thoroughly investigate and characterize the fluid dynamics of the Hele Shaw Model. This includes determining the model's limits of validity, examining the system's response to variations in the non-dimensional parameters governing the equations, and analyzing the dynamics during the fluid reinjection process. These objectives are conceived with the aim of being able to characterize what the reinjection of cold fluids would be like in highly confined environments.

The organization of this document is as follows: Chapter 2 provides a literature review on fault-controlled geothermal systems, reinjection in geothermal fields, the analogy of Hele-Shaw cells and porous media, and heat transport in Rayleigh-Bénard convection. In addition, scientific research questions, hypothesis, objectives, expected results, and the methodology will be presented. Chapter 3 provides a brief introduction and the article under preparation for submission. Chapter 4 presents additional results that were either not published or served as the starting point for developing the paper. Finally, Chapter 5 concludes the document with a summary of the findings, discussion of future work, and concluding remarks.

Chapter 2

Literature review

2.1. Fault-controlled geothermal systems and Reinjection in geothermal fields

To begin with, gaining a thorough understanding and characterization of geothermal reservoirs is crucial. In this regard, the research conducted by Moeck (2014) proves to be highly valuable. This study presents a comprehensive inventory of geothermal systems, categorized based on geological factors rather than just temperature and thermodynamic properties. Moreover, it introduces the concept of artificially *enhanced geothermal systems* (EGS), which refers to sites where the ratio between fluid temperature and flow rate is insufficient for economical utilization. To tackle this issue, technological solutions such as fluid injection or fracture generation are employed to enhance natural permeability and achieve the desired flow rate/temperature ratio. The most significant advantage of using this catalog is that direct measurements through an active observation well are not necessary. Key geological conditions, such as porosity, permeability, fracture patterns, and proximity to the heat source, play a pivotal role in determining the migration potential of geothermal fluids towards shallower levels in the crust.

We are interested in geothermal environments where advective heat transport dominates, as they are much more efficient compared to those dominated by conductive heat transport. According to Moeck (2014), it is possible to find this type of reservoir in active volcanic fields close to the magmatic chamber that act as a heat source, in places with active faults that allow the rapid migration of fluids, or in places that combine both characteristics: recent volcanic activity and active faults. An example of a fault-dominated reservoir can be seen in Figure 2.1. Most of the geothermal reservoirs exploited today correspond to reservoirs dominated by convective heat transport.

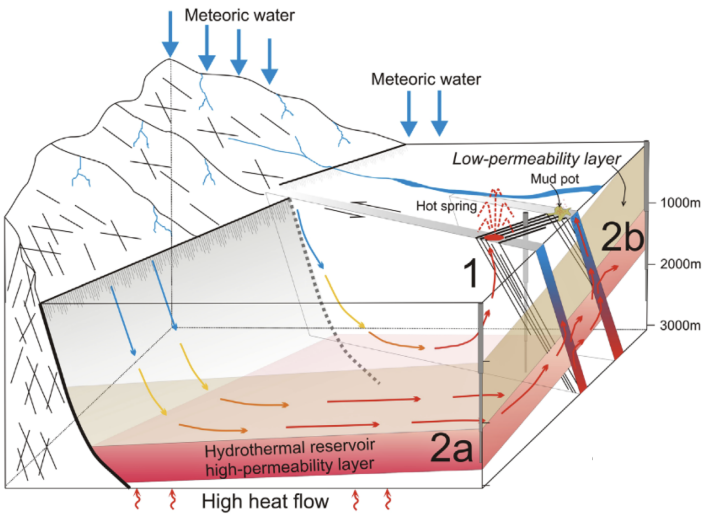

Figure 2.1: Non-magmatic geothermal system controlled by geological fault. Two types of reservoirs can be observed, (1) where all the flow dynamics occur along the same fault plane and (2) in which the fault acts as a leakage from the confined hydrothermal reservoir (the fault acts as a hydraulic connection between zones). Figure from Moeck (2014).

The practice of re-injecting reservoir fluids has become common nowadays, but it hasn't always been the case. In the 1980s, water extracted from geothermal reservoirs was often discharged into surface water bodies, posing environmental risks and affecting energy recovery. This discharge of geothermal water into surface water bodies posed a threat to the environment (Kamila et al., 2021). Geothermal waters generally contain components originating from two main sources. The first source is the magmatic fluids themselves, while the second source is the alteration caused by hydrothermal fluids in the porous matrix or source rock. For instance, in northern Chile, most thermal waters consist of brines with TDS (Total Dissolved Solids) exceeding 1000 [mg/L] (Risacher, Fritz, & Hauser, 2011). Because of this, wastewater injection in geothermal reservoirs was tested and put into practice.

Re-injection serves other purposes besides providing a solution for wastewater disposal. High extraction rates or lack of reinjection of geothermal fluid can affect system pressure, and a decrease in pressure can lead to intrusion of fluids from other aquifers into the reservoir (Shortall et al., 2015). Therefore, reinjection maintains reservoir pressure under control. It also provides the necessary recharge to maintain the fluid volume conditions in the reservoir that will eventually sustain geothermal exploitation.

Reinjection of fluids into geothermal reservoirs can have negative consequences. Reinjection can lead to several undesirable effects on steam production, such as chemical (problems with mineral deposition both in pipelines and in the porous matrix itself) or thermal breakthrough and boil-off suppression. In addition, reinjection may raise public concern about ground uplift, subsidence, and induced microseismicity (Kamila et al., 2021). The problem addressed in this study is geothermal breakthrough. This occurs when initial thermal and pressure conditions of the system are lost due to the injection of cold fluids. Also by injecting cooler water, the temperature will spread and reach the extraction zone, thus reducing the

temperature in the production wells and reducing the efficiency of the operation (Bödvarsson & Tsang, 1982; Pruess & Bodvarsson, 1984).

Kamila et al. (2021) has conducted a thorough review of re-injection practices in geothermal power plants, highlighting instances and direct occurrences of geothermal breakthrough. The paper highlights several instances of successful implementation of re-injection, including, for example, the Hellisheidi power plant in Iceland, which has an installed capacity of 303 $[MW]$ and generates equal amounts of power with an average reservoir temperature of 303 $[°C]$. In this plant, full reinjection (100% wastewater reinjection) is achieved through wells located at the reservoir's edges. The injection temperature typically ranges from $60-80$ $[°C]$, but can increase to $120-173$ $[°C]$ during thermal power plant maintenance, resulting in a rapid enthalpy change in wells located near the reinjection wells. This is a clear indication of thermal breakthrough. Moreover, it has been observed that the initial phase of wastewater reinjection at the Hellisheidi plant resulted in approximately 2 $[cm]$ of surface displacement, which can be linked to the pressure increases due to reinjection (Juncu et al., 2020). Another successful example is the Tuscarora plant in the USA, which also has a total reinjection scheme. After experiencing thermal breakthrough, the plant realized that one of the injection wells was strongly connected to the production zone, resulting in an initial decline of 3.5 $[°C]$ per year. By changing the problematic injection well, the plant achieved an almost immediate temperature recovery of 1.5 $[°C]$ and transitioned to a lower decline trend of 1.7 $[°C]$ per year (Chabora, Lovekin, Spielman, & Krieger, 2015).

Pruess and Bodvarsson (1984) developed an analytical solution to determine the time delay of the effects of cold water injection at a production point or well on vertical faults. The problem is characterized by several assumptions: a known geometry involving two parallel walls, a constant flow velocity, one-dimensional flow in a horizontal direction, heat conduction occurring only perpendicular to the flow, and specified initial and boundary conditions. It is obvious that this is a solution to an ideal problem where the assumptions may be far from reality, however, the paper highlights the effect of lateral conduction of heat from the reservoir rocks across the fracture faces on the faces. In an example given by the authors, the times could be several times shorter (3 times shorter in the example) if this effect of lateral heat conduction is not considered. Bödvarsson and Tsang (1982) also developed a similar model but for horizontal fractures, they also performed numerical tests to see the effect of the assumptions made, finding that not considering the heat conduction in the direction of flow can lead to errors in the temperature distribution at very late times.

Several numerical models have been developed in order to characterize the dynamics occurring at the time of reinjection (Blöcher et al., 2010; Saeid et al., 2013; T. Li et al., 2016; H. Liu et al., 2020), obtaining as results the characterization of the temperature drop of geothermal fluids in time and different thermal dynamics, depending on the context analyzed. Blöcher et al. (2010) made a 3D model of a geothermal research reservoir in Germany that has a doublet, i.e. an injection well and an extraction well. The model includes a complete hydrothermal coupling of several parameters, such as thermal conductivity and heat capacity as a function of temperature, as well as fluid density and viscosity as a function of pressure, temperature and mass concentration. The geological information available at the site is very rich. A Darcy flow model is solved in *FEFLOW*. The result of the model gives a time when the cold water front reaches the production wells (3.6 years) but it is

also interesting that the pressure perturbations traveled much faster and reach farther. Also that the hydraulic conductivity in the fractures depends strongly on the pore pressure of the system and that is something that the software they use manages to capture, however, they emphasize that the pore pressure can also vary due to the stress field, but that is something that they cannot incorporate.

Another example is Saeid et al. (2013) numerical model of a doublet in a deep geothermal reservoir that incorporates the wellbore, reservoir and surrounding soil components. The model solves a Darcy model in *COMSOL*. One of the peculiarities of this study is that it considers temperature-dependent viscosity and density variables. Among the results is the sensitivity of the model to viscocity and porosity, the higher the viscosity the propagation of the cold front slows down, and with the porosity, the higher the porosity of the matrix the faster the geothermal breakthrough.

As shown above, there are many models of cold fluid reinjection in geothermal reservoirs, which characterize the evolution of the temperature field as a function of time as well as the response that would be produced in these to variations of different parameters. *However, none of these models are direct numerical simulations and almost all use a Darcy model to describe flows in fractured or high-permeability zones, which can, as will be seen in later sections, overestimate heat fluxes.*

2.2. Hele-Shaw Model

A Hele-Shaw cell is a device commonly used in laboratory experiments to simulate the fluid flow through a porous medium. It consists of two parallel flat plates separated by a small gap, filled with a fluid. The gap between the plates can be considered as a simplified representation of a porous medium, as the fluid flow in the gap is restricted and controlled by the gap size and geometry, just like in a porous medium (Nield & Bejan, 2012).

The Hele-Shaw cell is particularly useful for studying the fundamental fluid flow and transport phenomena in porous media, such as Darcy's law, which describes the flow rate of a fluid through a porous medium (Saffman, 1986). The cell allows for direct visualization of the fluid flow patterns, making it easier to study the influence of various factors, such as fluid properties, pressure gradients, and geometrical features, on the flow behavior. Moreover, the Hele-Shaw cell is a cost-effective and versatile tool for conducting laboratory experiments on porous media, as it can be easily customized to simulate different types of porous media, such as sandstones, carbonates, or fractured media (Letelier et al., 2019; Ulloa & Letelier, 2022). Additionally, it allows for precise control of experimental parameters, such as the flow rate, temperature, and pressure, making it possible to obtain accurate and reproducible experimental results. In summary, the Hele-Shaw cell is a suitable laboratory model for porous media, as it provides a simplified yet realistic representation of fluid flow in porous media and allows for detailed experimental investigation of flow behavior and transport phenomena.

Within a Hele-Shaw cell with a gap width of b, the relationship between the two-dimensional averaged velocity u of a viscous fluid confined between the cell walls and the pressure p is

governed by a set of equations 2.1. These equations are derived from the Navier-Stokes equations and the continuity equation (Saffman, 1986):

$$u = \frac{b^2}{12\mu}(-\rho g\hat{k} - \nabla p) \qquad \nabla \cdot u = 0 \tag{2.1}$$

Where μ is the dynamic viscosity of the fluid, ρ is the density of the fluid, g is the acceleration of gravity and $\hat{k}$ is the unit vector pointing in the same direction as gravity. The above relationship is identical to Darcy's law in a porous medium of permeability $K = b^2/12$. Evidently, this is an approximation that is valid when the ratio between the separation b and the cell height H is small and gets worse as this ratio increases. Figure (2.2) shows a representation of the Hele Shaw cell analogy.

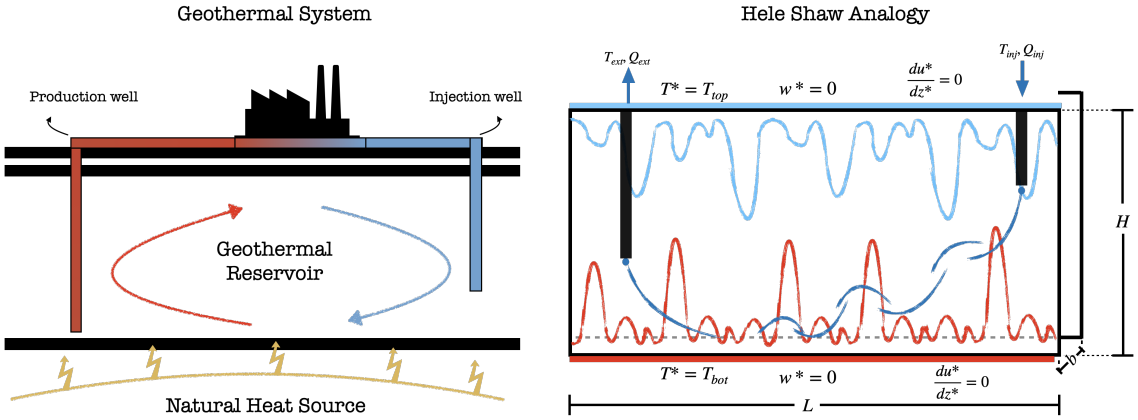

Figure 2.2: Geothermal system schematic of a doublet and its representation with the Hele Shaw analogy. In the Hele Shaw representation there are boundary conditions of constant temperature at top and bottom, free slip and no penetration.

Letelier et al. (2019) recently conducted an investigation into buoyancy-driven flows in Hele Shaw cells, using a combination of perturbation techniques and numerical simulations to examine the impact of Rayleigh number and cell anisotropy on flow behavior. Letelier et al. (2019) derived a 2D model that takes into account both inertial corrections in the momentum equation and mechanical dispersion in the scalar transport equation to describe thermal convection in a Hele Shaw cell. The Hele Shaw Model (HSM), results from averaging the Navier-Stokes equation and the advection-diffusion model for heat transport in the confinement direction. The latter can be considered as a correction of the advection-diffusion model for heat transfer and Darcy equation, incorporating inertial and dispersive terms proper to the cell geometry.

Their findings revealed the presence of three distinct flow regimes, in agreement with the $\epsilon^2 Ra$ parameter value: (i) the Darcy regime ($\epsilon^2 Ra \to 0$), in which the flow is two-dimensional and can be accurately described using Darcy simulations; (ii) the Hele-Shaw regime ($\epsilon^2 Ra \ll 1$), in which the flow remains two-dimensional but is influenced by gap-induced dispersion, and (iii) the three-dimensional regime ($\epsilon^2 Ra \gg 1$), where the effects of the third dimension become significant. *The exact range of validity of the set of equations introduced by Letelier et al. (2019) has not yet been established.* In summary, the Hele-Shaw

regime is an intermediate regime between two and three dimensions, but the mathematical formulation is still two dimensional. It's important to note that the source of hydrodynamic dispersion in a Hele-Shaw cell differs from that in porous media. In the latter, flow path tortuosity and friction with the solid matrix's surface result in fluid and solute following meandering paths. This mechanical dispersion causes additional mixing and dilution effects and is responsible for the Ra dependent behavior of dissolution rate (Liang, Wen, Hesse, & DiCarlo, 2018). In contrast, Hele-Shaw flow's dispersion is produced by the presence of a constrained third dimension (Taylor hydrodynamic dispersion).

It is worth noting that De Paoli, Alipour, and Soldati (2020) conducted experiments to validate Hele-Shaw regime observed by Letelier et al. (2019) in numerical simulations, in which different openings of the Hele-Shaw cell were tested. De Paoli et al. (2020) work further refined the boundaries of the Hele-Shaw regime, defining them as being between $0 < \epsilon^2 Ra < 1$ and the three-dimensional regime $1 \leq \epsilon^2 Ra$. Due to the fact that conductivity is directly linked to cell anisotropy, a fractured porous medium could be in the Hele Shaw regime, so estimating parameters and fluxes only with Darcy's law could be giving erroneous results. The effect it has on heat transport and the mathematical model is discussed in Section 2.3.

2.3. Heat transfer in RBC

Heat transport by convection, i.e. fluid motion due to gravity acting on an unstable density profile, is an interesting problem that appears in a large number of earth science problems. For example, it is the mechanism responsible for the transport of heat in the atmosphere by the upward transfer of heat absorbed in the soil. It is also responsible for the mixing of water masses in the oceans (Gauthier et al., 1978). In porous media, heat from the Earth's core drives subsurface hydrothermal convection that can be harnessed as geothermal energy (Letelier et al., 2019; Hewitt, 2020). Salt concentration gradients in the subsurface can also drive convection (Evans & Nunn, 1989). Convection results in increased scalar transport and also has an effect on fluid mixing.

Rayleigh Bénard Convection (RBC) consists of a fluid confined between two parallel plates at constant temperature such that the temperature of the lower plate T_{bot} is higher than the temperature of the upper plate T_{top}. Due to buoyancy effects, when the temperature difference between the plates exceeds a critical value T_{crit}, the state of conductive immobility is unstable and convection occurs (Bodenschatz et al., 2000). Clearly, the flow dynamics that occur between these plates are not the same if we compare a free fluid with what happens in a porous medium. In porous media, the presence of solid particles or other obstructions can significantly affect the flow patterns and heat transfer characteristics (S. Liu et al., 2020). The porous medium can act as a filter or restrictor, creating additional resistance to fluid flow and affecting the onset and stability of the convective motion. Rayleigh-Bénard convection in porous media has important applications in geosciences, such as the study of natural convection in the Earth's mantle (Mckenzie, Roberts, & Weiss, 1974; Yan, Ballmer, & Tackley, 2020), and in engineering, such as the design of geothermal energy systems and enhanced oil recovery (Blöcher et al., 2010; H. Liu et al., 2020).

As discussed in Section 2.2, the Hele Shaw regime is an intermediate step between the porous medium regime and a fully 3D problem. This is why remarkable results of RBC in 3D free fluids and in porous media will be reviewed.

One of the most important works on Rayleigh Bénard convection in 3D is the one done by Ahlers et al. (2009). They made a compilation of theoretical, experimental and numerical studies on 3D Rayleigh Bénard convection. The most commonly used mathematical approximation consists of using the Oberbeck-Boussinesq approximation in which the density ρ of the fluid depends linearly on the temperature:

$$\rho(T) = \rho(T_0)\left[1 - \beta(T - T_0)\right] \tag{2.2}$$

Where β is the thermal expansion coefficient. Most models also consider the coefficient of thermal expansion β, kinematic viscosity ν, and thermal diffusivity κ to be constant. Then the governing equations of RBC are (if we consider a closed container of height H):

$$\partial_i u_i = 0 \tag{2.3}$$

$$\partial_t u_i + u_j \partial_j u_i = -\partial_i p + \nu \partial_j^2 u_i + \beta g \delta_{i3} \theta \tag{2.4}$$

$$\partial_t \theta + u \partial_j \theta = \kappa \partial_j^2 \theta \tag{2.5}$$

Where $u(x,t)$ is the velocity field, $p(x,t)$ is the pressure, θ is the temperature field relative to some reference temperature, g is the gravitational acceleration, and δ_{ij} is the Kronecker delta. Here all variables are dimensional. Typical boundary conditions of the problem are $u = 0$ at the walls (no slip condition), $\theta(z = -H/2) = \Delta T/2$ and $\theta(z = H/2) = -\Delta T/2$, at the sidewalls no lateral heat flow. The equations of motion are determined by 2 dimensionless parameters, Rayleigh Number, Prandtl Number. In addition, there is an important dimensionless number that is the aspect ratio of the geometry:

$$Ra_{3D} = \frac{\beta g H^3 \Delta T}{\kappa \nu} \qquad Pr = \frac{\nu}{\kappa} \qquad \Gamma = \frac{b}{H} \tag{2.6}$$

The parameter b depends on the geometry in which the experiments are made. In a cubic cell b represents the width, in a cylindrical cell b represents the diameter of the cell. Rayleigh number Ra characterizes the transport regime (convective or conductive) and is defined as the ratio between buoyant and diffusive effects, in addition, this number can be thought of as the ratio of the timescale to diffuse a distance H to the timescale to convect over that distance. The Prandtl number Pr is the ratio of momentum diffusivity to thermal diffusivity, this parameter measures the relative importance of the nonlinear terms in the equations of motion, also has a direct relationship with the boundary layers of the system (Bodenschatz et al., 2000). The response of the system is measured with the Nusselt Number. The Nusselt number (Nu) is a crucial dimensionless parameter used in fluid mechanics and heat transfer to determine the principal response of a system, particularly in describing the convective heat transfer between a fluid and a solid surface. This parameter provides a way to relate the convective heat transfer coefficient to the thermal conductivity and the characteristic length scale of the system, making it an essential tool for predicting the heat transfer rate from a heated surface to a fluid or from a fluid to a cooled surface. It is calculated as:

$$Nu = \frac{\langle u_z \theta \rangle_A - \kappa \partial_3 \langle \theta \rangle_A}{\kappa \Delta T H^{-1}} \tag{2.7}$$

Where $\langle \cdot \rangle_A$ denotes the average over any horizontal plane and over time. The flow in these systems reach a statistically stable state, which allows the investigation of heat fluxes (Le Reun & Hewitt, 2021). The main idea is to find the relationship between the Nusselt number and the dimensionless numbers that dominate the problem, i.e. the Rayleigh number, the Prandtl number and the aspect ratio. Although it is known that there is a dependence of the system on the aspect ratio, the old theories and the theory postulated by Grossmann and Lohse do not incorporate a direct dependence.

The older scaling theories for the Nusselt number typically take the form of $Nu = Ra^{\alpha} Pr^{\beta}$. The values of the exponents depend on the assumptions made, with the Rayleigh exponents varying between 1/2 and 1/4, and the Prandtl exponents between 1/2 and -1/4. However, these scaling laws did not offer a unified perspective and often did not agree with experimental measurements. One of the major discrepancies was the dependence on the Prandtl number, which differed significantly with observed data. To address this issue, Grossmann and Lohse (2000) developed a unifying theory for estimating the Nusselt number, Nu(Ra,Pr), over a wide range of dimensionless parameters.

Grossmann and Lohse's theory divides the domain into two parts: the bulk and the boundary layers, since the physics in each region is fundamentally different. The authors emphasize the importance of the relative thickness between the thermal boundary layer and the kinetic boundary layer. In regimes with low Prandtl numbers, the kinetic boundary layer is contained within the thermal layer, while in high Prandtl regimes, the opposite is true, leading to a different approach to modeling the thicknesses of the boundary layers. The scaling of the Nusselt number depends on the dominant region and the relationship between the boundary layers (all escalations factors can be reviewed in Grossmann and Lohse (2000)).

It is worth noting the concept of the Ultimate Regime or asymptotic heat transfer, which occurs when the heat transfer and turbulence strength become independent of kinematic viscosity and thermal diffusivity. This means that the thermal boundary layer and kinetic boundary layer no longer significantly affect heat fluxes, and the flow is dominated by the bulk. In this regime, Grossmann and Lohse's theory proposes that if the thickness of the kinetic boundary layer exceeds that of the thermal boundary layer (a high Pr regime), the scaling of the Nusselt is $Nu \sim Ra^{1/3}$ (Grossmann & Lohse, 2001; Ahlers et al., 2009). For low Pr regimes, where the opposite is true, the scaling is $Nu \sim Ra^{1/2} Pr^{1/2}$. This highlights the critical role played by boundary layer thickness and suggests that the Nusselt scaling depends on the ratio of kinetic to thermal boundary layer thickness.

Additionally, Bhattacharya, Verma, and Samtaney (2021) conducted a study on 3D RBC and found that the Prandtl number also influences the local heat flux fluctuations. A higher Prandtl number leads to convection occurring through increasingly thinner thermal plumes, resulting in stronger fluctuations and inhomogeneity in the heat flux.

Recently, two studies (Chong & Xia, 2016; Chong, Wagner, Kaczorowski, Shishkina, & Xia, 2018) have shown that extreme one-dimensional confinement (i.e., very low Γ) can lead to changes in the classical scaling laws. In Chong and Xia (2016), the behavior of Rayleigh–Bénard convection in the severely confined regime was investigated using direct

numerical simulations (DNS), solving equations 2.3, 2.4 and 2.5 with the conditions of no slip and impermeability applied to all walls and adiabatic conditions at the sidewalls, while the top and bottom walls are maintained at a constant temperature. The authors defined the severely confined regime as when the distance between the plates is only a few times the thermal boundary layer thickness, which is significantly smaller than the standard geometrical confinement for Rayleigh–Bénard convection. In this paper, the Prandtl number is fixed at 4.38, while Rayleigh is varied from 10^4 to 10^{11} and Γ is varied from 1 to 1/128.

The primary outcome of this paper is illustrated in Figure 2.3. The authors performed simulations, which revealed that in the severely confined regime, plumes continue to dominate heat transfer, but the plume structures undergo significant alterations. The heat transfer efficiency was found to be higher than predicted by classical scaling laws. The authors also observed that the heat transfer enhancement in the severely confined regime was due to the formation of coherent structures near the walls, referred to as wall-to-wall megaplumes, when the aspect ratio Γ was small. This behavior is similar to the creation of coherent structures in a 2D free fluid that flows through obstacles which simulate a porous medium, improving heat transport (S. Liu et al., 2020). Chong and Xia (2016) also demonstrated that for high Ra regimes, the Nusselt number collapses into a straight line, regardless of the value of Γ. Additionally, numerical simulations confirmed that the onset of convection agreed with theoretical predictions derived for Hele Shaw cells (Bizon, 1997).

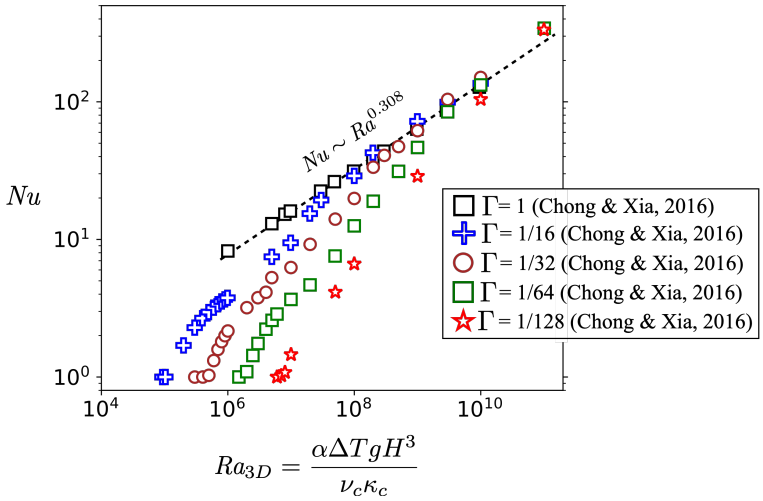

Figure 2.3: Nusselt vs Rayleigh results for various gamma values. It is worth noting that at high Rayleigh numbers, the Nusselt number tends to collapse in a straight line that fits the results for $\Gamma = 1$. Modified from Chong and Xia (2016).

The other study, Chong et al. (2018), investigates the effect of varying the Prandtl number on heat transport in confined media. The setup and boundary conditions are the same as in the previous study. This time, a Rayleigh number of 10^8 is fixed, while the Prandtl number is varied between 0.1 and 40, and Γ between 0.025 and 0.25. Figure 2.4 shows the Nusselt number results. Among the main conclusions is that a very weak dependence on Nusselt is observed for large Pr, a result also described by Ahlers et al. (2009) and Shishkina, Emran, Grossmann, and Lohse (2017). Another characteristic they found is that when the ratio

of the thermal boundary layer thickness λ_T to the momentum thickness λ_p is around one, an optimal coupling is generated between the normal stress and temperature fluctuations, leading to optimal heat transport. For $Pr < 0.5$, the Nusselt number is decreased. X. M. Li, He, Tian, Hao, and Huang (2021) also reports a similar study in confined environments, however the Γ values are too high to compare with a Hele Shaw model.

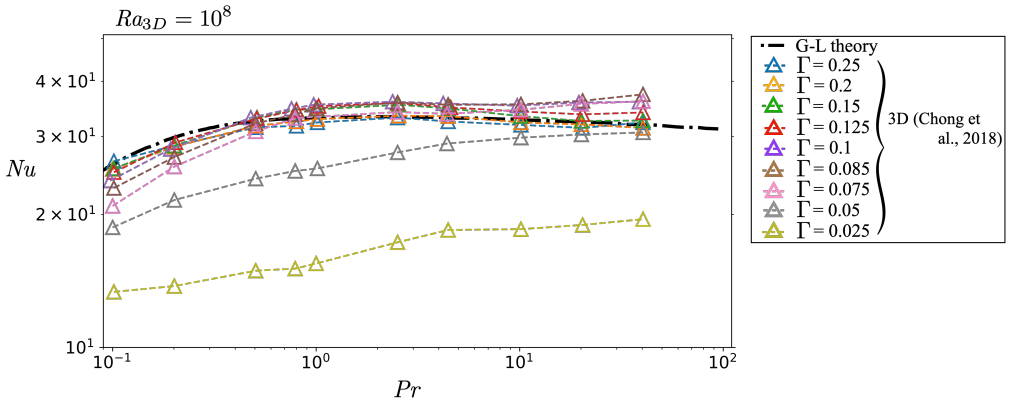

Figure 2.4: Nusselt vs Pr results for various gamma values. The black dashed line is the Pr dependence of Nu estimated by Grossmann-Lohse theory. Modified from Chong et al. (2018).

The two studies presented in detail, Chong and Xia (2016) and Chong et al. (2018) are a fundamental pillar for this investigation. As seen in the previous section, a Hele-Shaw cell is precisely an apparatus in which the width-to-height aspect ratio Γ is very low. *The value of these studies lies in the fact that the solved equations are in three dimensions, whereas the Hele-Shaw model is a 2D model that incorporate information about the confined dimension.* Therefore, the results of these studies are useful for comparison and for establishing the limits of the Hele-Shaw model.

On the other hand, the problem in porous media is slightly different, starting with the equations that model the phenomenon. The flow in porous media is typically modeled through continuum modeling, which involves averaging relevant quantities such as pressure, density, and velocity over a representative volume that encapsulates many pores (REV) (Nield & Bejan, 2012). This approach allows the flow to be described in terms of the mean volume flux or Darcy velocity u. Instead of resolving the Navier-Stokes equation, in porous media, Darcy's law is valid, which relates the driving pressure and buoyancy forces to the viscous drag imparted by the medium's pore scale (Hewitt, 2020). Using the Oberbeck-Boussinesq approximation the equations are:

$$\partial_i u_i = 0 \tag{2.8}$$

$$\mu K^{-1} u = -\partial_i p + \rho g \delta_{i3} \tag{2.9}$$

$$\partial_t T + u \partial_j T = \kappa \partial_j^2 T \tag{2.10}$$

Here K is the permeability of the medium, ρ is the fluid density and μ is the dynamic viscosity. Unlike free fluids, here the only dimensionless control parameter is the Rayleigh number. Although they have the same meaning, the mathematical formulation is different.

$$Ra = \frac{\beta \Delta T g K H}{\kappa \nu} \tag{2.11}$$

Because the system of equations is a little simpler to solve than that of free fluids, there are more theoretical studies. Linear stability analysis shows that in a 2D Rayleigh-Bénard cell, if the Rayleigh number is less than the critical Rayleigh number $Ra_{crit} = 4\pi^2$, a vertically linear and horizontally uniform temperature field is stable. This means that the effects of diffusion and viscosity are too significant, and no flow occurs, resulting in the transfer of buoyancy being entirely diffusive, above that Rayleigh number instability appears as convection (Nield & Bejan, 2012).

Above the critical Rayleigh number, two distinct regimes can be identified: the low Rayleigh regime and the high Rayleigh regime. Studies have investigated these regimes in 2D porous media (Palm, Weber, O D D M U N, & Kvernvold, 1972; Otero et al., 2004; Hewitt et al., 2012). In contrast to what occurs in free fluids, in the mathematical formulation of porous media, there is no Prandtl number. This leads to fewer difficulties compared to those for free fluids.

In the low Rayleigh regime, stable plumes form, and small instabilities grow in the vicinity of boundary layers that are not strong enough to disrupt the system's order. The Nusselt number in this regime does not exhibit a clear scaling behavior. In porous media, for approximately $Ra > 1250$, there is a decrease in heat transport due to the reordering of structures caused by the growing significance of instabilities in the boundary layers (Hewitt, 2020). This marks the transition between the low Rayleigh regime and the high Rayleigh regime.

In the high Rayleigh regime, the flow within the cell is dominated by vertical exchange flow consisting of interleaving columns of hot and cold fluid with a horizontally varying wavelength dependent on Ra. Heat is transferred through thin diffusive boundary layers at the upper and lower boundaries, which are unstable and give rise to the growth of short-wavelength and intermittent plumes. Between the relatively ordered interior flow and the boundary layers, there is a region characterized by intense mixing and transient flushing of these short-wavelength plumes, as heat is exchanged between the boundary layers and the interior exchange flow. In the high Rayleigh regime, the scaling relationship is sublinear, with $Nu \sim Ra^{0.9}$ (Otero et al., 2004; Hewitt et al., 2012). However, in the theoretical limit as Ra tends to infinity, it is expected that the relationship between the Nusselt number and the Rayleigh number approaches linearity, $Nu \sim Ra$. This can be understood using dimensional analysis, where heat transport is determined by the marginal stability of the thermal boundary layers and the mean temperature gradient (Malkus, 1954). Figure 2.5 shows the results obtained by Hewitt et al. (2012). In 3D simulations in porous media (Hewitt, Neufeld, & Lister, 2014), it has been observed that the scaling for high Rayleigh regimes remains the same, i.e., $Nu \sim Ra$, with the exception that the prefactors change in the exact relationship (De Paoli, Pirozzoli, Zonta, & Soldati, 2022).

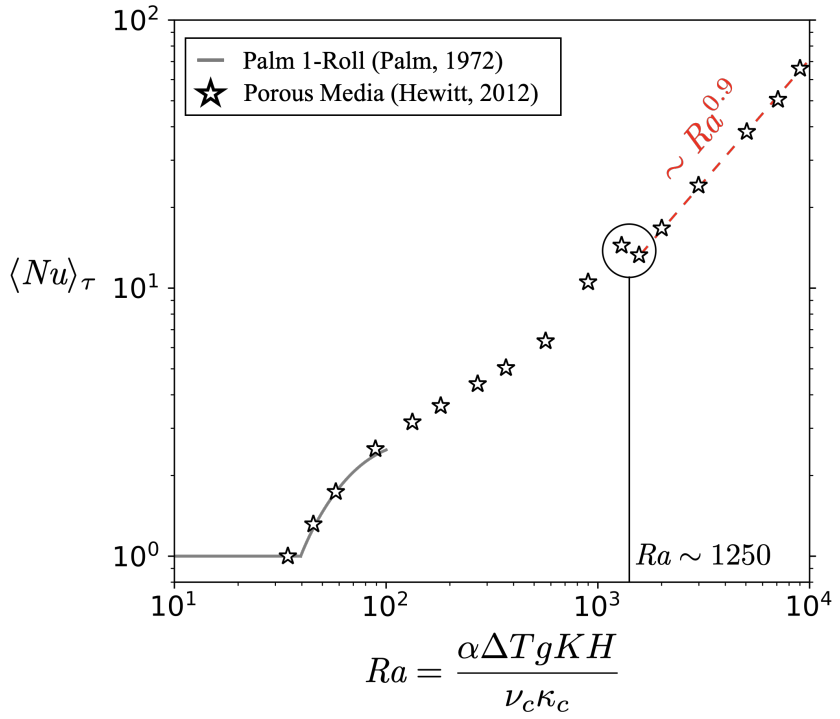

Figure 2.5: Nusselt vs Ra results porous media obtained by Hewitt et al., (2012). With gray line Palm et al., (1972) theoretical results can be observed. The clear transition between high Rayleigh and low Rayleigh regimes can be observed.

Otero et al. (2004) investigated the presence of a hysteresis effect on a 2D porous media model, as evidenced by the star-marked curve in Figure 2.6. They conducted simulations with descending Ra values, starting from an initial condition corresponding to a higher Ra simulation. Within the range of $160 < Ra < 1000$, three stationary convective cells are favored, contrasting with the single pair observed in the ascending Ra simulations. The Nusselt number exhibits a higher value in certain ranges and a lower value in others. In this Ra range, the scaling of Nu is lower compared to the ascending Ra trajectory. As Ra is reduced below 160, the solution transitions to the formation of two convective cells, leading to a significant enhancement in heat transport. Finally, within the range of $50 < Ra < 76$, the solution favors the formation of a single convective cell, accompanied by an increase in heat transport. This effect is important when analyzing results because, essentially, for the same Rayleigh number, there are at least two states in which steady states can be reached, leading to different Nusselt number outcomes.

The hysteresis effect also has been observed in laboratory experiments on porous media. Murray and Chens (1989) conducted an experiment on a horizontal layer of porous medium to study double diffusive convection involving both mass and heat transfer. They observed hysteresis by increasing the Rayleigh number beyond the critical value and then decreasing it below the critical value. This led to different paths in the heat fluxes, indicating the existence of hysteresis loops in the system.

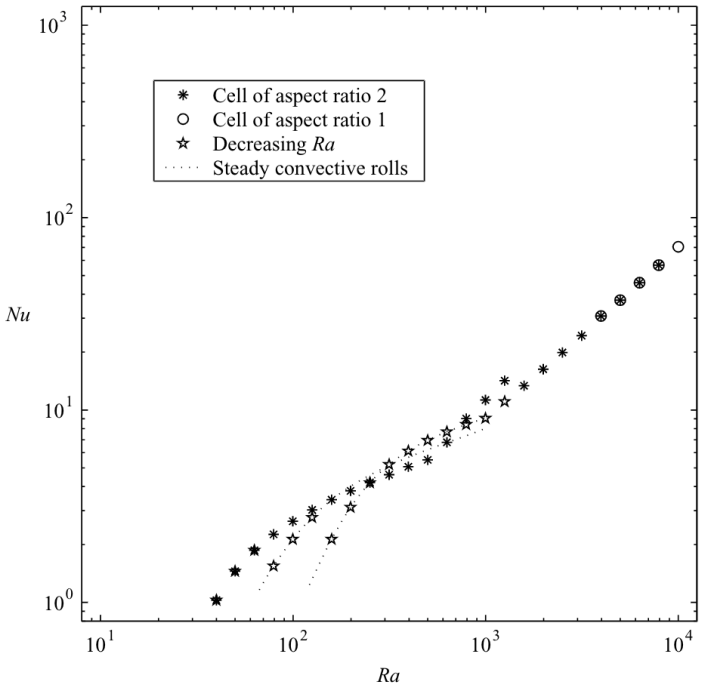

Figure 2.6: Nu vs Ra in porous media obtained by Otero et al. (2004). The data from the run with increasing Ra is shown together with data for the run in which Ra was decreased from $Ra = 1255$, indicated by stars. The heat transport for the 2-pair and 3-pair steady roll solutions is shown by the dotted line. Figure from Otero et al. (2004)

The influence of the Prandtl number on flow behavior in porous media has been relatively overlooked, primarily due to its absence in the classical Darcy formulation, as mentioned. Jonsson and Catton (1987) conducted a study involving both numerical simulations and experimental investigations in porous media with fluids of varying Prandtl numbers. They observed that the results exhibited variations depending on the effective Prandtl number (Pr_e), which is determined by the fluid properties and porous media properties, particularly for values below $Pr_e < 0.1$. Below this limit, the Nusselt number decreases, indicating a reduction in heat transport efficiency. Conversely, above this limit, the Prandtl number seems to have no discernible effect on heat transport. The numerical simulations were performed by adding the Darcy model with a Brinkmann term and the Forcheimer term.

Wang and Bejan (1987) demonstrated that the spread of the experimental data could be significantly reduced by considering the effect of fluid inertia by taking into account the quadratic drag included in the Forcheimer term, which becomes increasingly significant as the Rayleigh number increases. They utilize a dimensionless number Pr_p, obtained by multiplying the effective Prandtl number by the Darcy number, to analyze the equations. Upon examining the magnitudes of the terms in the equations, the authors identify three distinct regimes. The first is the subcritical (conduction) regime, characterized by $Ra < 40$, where $Nu = 1$. The second is the Darcy convection regime, with $40 < Ra < Pr_p$, where Nu follows the classical Darcy scaling, depending only on Rayleigh number. The third regime is the Forcheimer convection regime, occurring for $Ra > Pr_p$, where Nu decreases in comparison to the Darcy regime, depending on Ra and Pr_p. Figure 2.7 illustrates a schematic representation of these regimes. This is similar to what was obtained by Letelier et al. (2019) when investigating

the effect of incorporating inertial and hydrodynamic dispersion corrections. However, these corrections and the Forchheimer term are quite different.

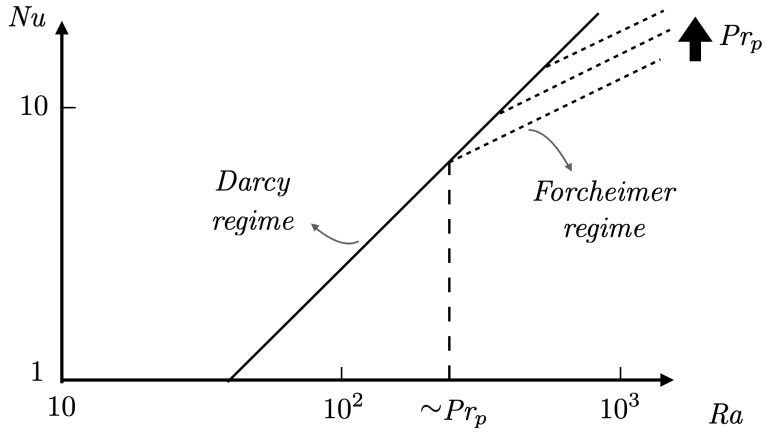

Figure 2.7: Scheme of the regimes studied by Wang and Bejan (1987). Modified from Wang and Bejan (1987).

Another effect that is important to note in porous media is dispersion. Dispersion in porous media is a significant phenomenon that has been widely studied in the literature (Bear, 1967; Sahimi & Imdakm, 1988; Puyguiraud, Gouze, & Dentz, 2021). However, previous works often neglected this effect in their investigations (Otero et al., 2004; Hewitt et al., 2012). In general, the dispersion of substances or particles in a porous medium is attributed to two main factors: molecular diffusion and convective dispersion, also known as mechanical dispersion. The combined effect of these processes is referred to as hydrodynamic dispersion (Nguyen & Papavassiliou, 2020). The dispersion process is influenced by various factors, including the pore structure, flow velocity, molecular diffusion, and molecular interactions. Although hydrodynamic dispersion is a macroscopic phenomenon, its underlying causes lie in the complex microstructures of the porous media and the non-uniform microscopic movement of the fluid. To fully understand hydrodynamic dispersion, a microscopic analysis of the system is necessary (Sun, 1996).

Wen, Chang, and Hesse (2018) conducted a study on a Darcy model with longitudinal and transverse dispersion. They discovered that in a sufficiently wide domain, the dynamics of the system are governed by three key parameters: the molecular Rayleigh number Ra_m (same as 2.11), the dispersive Rayleigh number Ra_d, and the dispersivity ratio r. When mechanical dispersion dominates as the primary dissipative mechanism, the convective flux is mainly controlled by Ra_m, while the convective pattern is determined by Ra_d. This implies a decoupling between convective flux and pattern during porous media convection with dispersion. Furthermore, the study by Wen et al. (2018) confirmed that the linear flux scaling relationship, $F \sim Ra_m$, obtained in previous works remains valid even in the presence of hydrodynamic dispersion. However, it was found that the prefactor of this relationship is determined by Ra_d, the dispersive Rayleigh number. This indicates that while mechanical dispersion dominates as the primary dissipative mechanism, the convective flux is still governed by Ra_m, but the magnitude of the flux is influenced by Ra_d. Therefore, Ra_d plays a crucial role in determining the specific value of the prefactor in the linear flux scaling relationship.

As discussed in Section 2.2, the Hele Shaw model is particularly suitable for studying porous media with a high permeability coefficient, such as fractured media. In the case of a vertical fracture, Murphy (1979) investigates natural convection of water in a vertical fracture or fault where the temperature increases with depth on a Darcy model. The heat transport process is influenced not only within the water itself but also by heat exchange with the surrounding rock mass. The findings from a linear stability analysis reveal that the critical Rayleigh number, Ra_c, which characterizes the onset of convection, is time-dependent and in general, is several orders of magnitude higher than the value that would apply to a porous bed without the influence of the surrounding rock mass.

Malkovsky and Magri (2016) conducted research on the onset of thermal convection in a single-phase fluid with temperature-dependent viscosity in a vertical permeable fault. The study utilized a 3D Darcy model and employed linear stability analysis and numerical simulations. It was observed that the decrease in the critical Rayleigh number is influenced by the dimensionless number that represents the viscous property of the fluid. Interestingly, the destabilizing effect of temperature-dependent viscosity on thermal convection in the fault was found to be independent of the fault width. The study also revealed that in faulted geothermal systems, thermal convection can occur within faults with permeability up to 4 times lower than that of a fluid with constant viscosity. Moreover, the variable fluid viscosity effects dominate over the stabilizing thermal feedbacks of the surrounding rocks, even when there is enhanced heat exchange between the fault and conductive rocks due to thermal conductivity heterogeneity. This research highlights the significance of fluid viscosity effects in faulted sedimentary basins, suggesting that thermal convection may have been underestimated in previous studies that neglected these effects.

The studies conducted by Murphy (1979) and Malkovsky and Magri (2016) provide valuable insights into the intricate nature of real-world situations, emphasizing the complexity and multitude of variables and effects involved. They serve as a reminder of the significance of avoiding oversimplified upscaling approaches when working with data obtained from laboratory experiments or numerical simulations that rely on idealized assumptions. Failing to account for the intricate ways of the real system can result in misleading or inaccurate outcomes.

The phenomenon of Rayleigh-Bénard convection (RBC) has also been investigated in the context of Hele-Shaw flow. Notably, Aniss, Souhar, and Brancher (1995) conducted an important study in this area. They employed dimensional analysis and the Hele-Shaw approximation, utilizing classical asymptotic methods. As a result, they were able to identify two distinct nonlinear formulations of the original problem, with each formulation dependent on the Prandtl number's order of magnitude. This finding highlights the Prandtl number's control over the weakly nonlinear aspects and the thermal-hydrodynamic characteristics of modes. Aniss et al. (1995) further concluded that as the aspect ratio Γ approaches zero, the analogy between 2D porous media and Hele-Shaw cells becomes more rigorous. The influence of the Prandtl number becomes pronounced when it is low, particularly the authors set it when $Pr = O(\Gamma^2)$ is considered. In this scenario, the nonlinear contributions $v \cdot \nabla T$ from the energy equation result in the persistence of advection terms $v \cdot \nabla v$ in the equations of motion for the Hele-Shaw approximation. Therefore, it becomes misleading to draw an analogy between flow in porous media and flow in the Hele-Shaw cell. Consequently, the

Prandtl number plays a crucial role in determining the amplitude equation and influencing its coefficients.

Recently, Letelier et al. (2019) conducted a study that investigates the significance of dispersive terms and perturbative corrections in Hele Shaw cells on Rayleigh Benard Convection. This work focuses on establishing a physical model by applying perturbative corrections to the Navier-Stokes equations in a quasi-3D domain. This model is derived from fundamental physical principles, specifically the continuity equation, Navier-Stokes equation, and advection-diffusion equation, which are averaged within the gap of the Hele-Shaw cell. In Figure 2.8, a schematic diagram of the conceptual model can be observed. As mentioned before, direct analogies can be made between Hele-Shaw cells and porous media, specifically incorporating corrections that account for hydrodynamic dispersion and inertial effects in Darcy's law. The dimensionless equations are presented below:

$$\partial_i u_i = 0 \tag{2.12}$$

$$\epsilon^2 \frac{Ra}{Pr}\left(\frac{6}{5}\partial_t u + \frac{54}{35}u_j\partial_j u_i\right) = -\partial_i p - u_i + T\delta_{i3} + \frac{6}{5}\epsilon^2\delta_j^2 u_i - \frac{2}{35}\epsilon^2 Ra(u_j\partial_j T)\delta_{i3} \tag{2.13}$$

$$\partial_t T + u_i\partial_i T = \frac{1}{Ra}\partial_i^2 T + \frac{2}{35}\epsilon^2 Ra\,\partial_j((u_i\partial_i T)u_j) \tag{2.14}$$

The study investigates the scaling behavior of the Nusselt number and the thermal dissipation rate as a function of dimensionless parameters, including the Rayleigh number, cell anisotropy ϵ ($\epsilon = \Gamma/\sqrt{12}$), and Prandtl number. As depicted in the equations, unlike in 3D free convection or porous media, the Hele-Shaw Model (HSM) set explicitly includes a dimension parameter associated with the geometry, denoted as ϵ. The Hele-Shaw equations are applicable when ϵ is small, Pr is greater or equal to 1, and $\epsilon^2 Ra$ is much smaller than 1. As ϵ approaches zero, and with a fixed Ra, the model simplifies to the Darcy equations coupled with the advection-diffusion model. *The exact range of validity of this set of equations is still not clear.* Numerical simulations were conducted to analyze the fluid dynamics of heat transport using a 2D model specifically designed for vertical Hele-Shaw geometries. The findings highlight that incorporating mechanical dispersion and inertial effects in the porous media model yields new scaling relationships for heat transport and total thermal dissipation in the high-Ra regime, particularly valid for cases where $\epsilon^2 Ra << 1$.

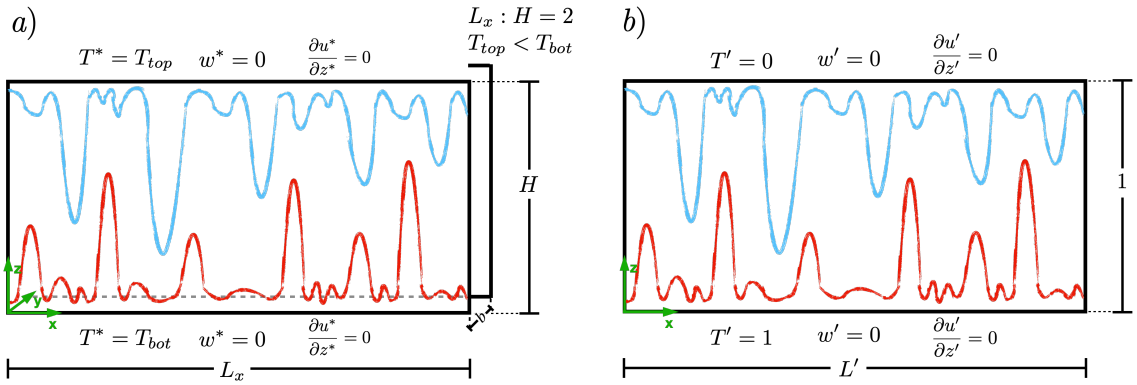

Figure 2.8: a) Hele-Shaw cell model with its respective boundary conditions. b) Dimensionless representation of the problem.

The main result is shown in Fig 2.9. It can be observed that for low Rayleigh regimes, for the two simulated cell anisotropies, the perturbative and hydrodynamic dispersion corrections do not affect the heat transport, emulating the same results obtained for porous media. However, starting from $Ra \sim 1350$, there is not only a deviation of the results from those of porous media but also between the two simulated cell anisotropies. This demonstrates that heat transport, or consequently, the Nusselt number, depends on the anisotropy and is affected by hydrodynamic dispersion and perturbative corrections. In particular, as ϵ increases, there is a greater amount of dissipated heat, increasing the importance of the added corrections, which causes the scaling of the Nusselt number decreases as a function of ϵ. Letelier, Herrera, Mujica, and Ortega (2016) and Noto, Ulloa, and Letelier (2023), in the context of laboratory experiments in Hele-Shaw cells, observe that one-dimensional spatial confinement has an effect on overall heat transport. This provides support for the use of this model and motivates a better understanding of the physics of heat transport in confined environments.

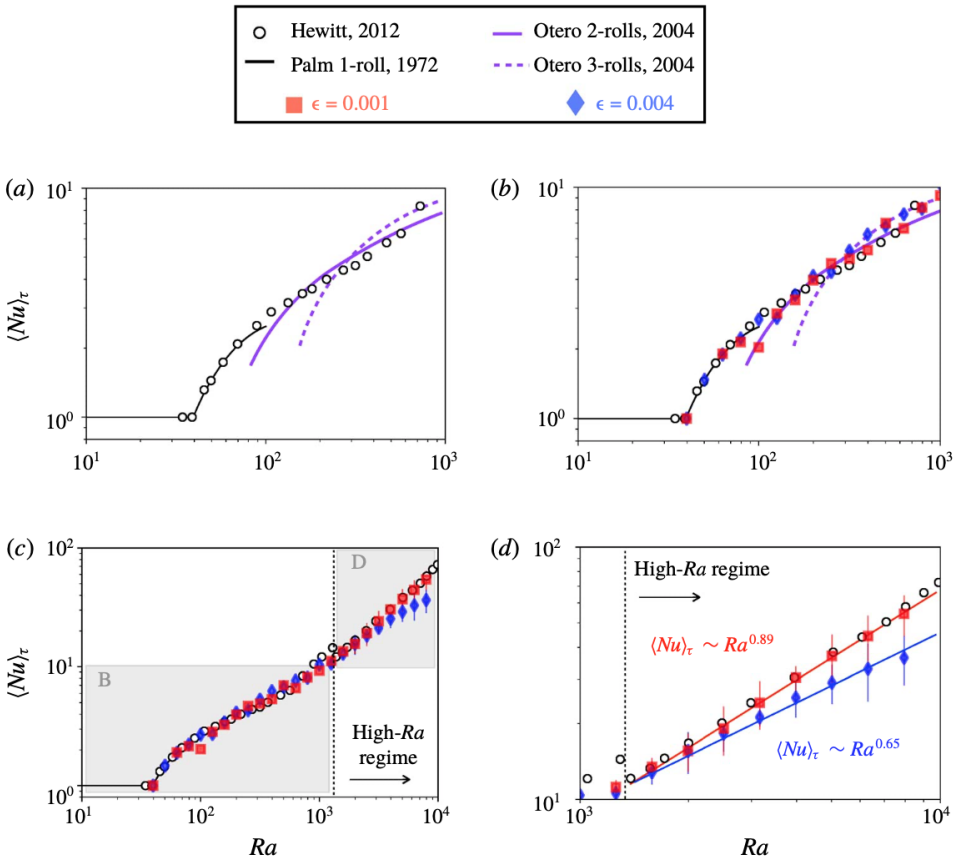

Figure 2.9: The Nu-Ra relationship obtained in this study is compared to findings from other studies in the literature for models with $\epsilon = 0.001$ and $\epsilon = 0.004$. Differences in scaling are observed for high Rayleigh numbers ($Ra > 1350$) due to the incorporation of inertial and hydrodynamic dispersion corrections. Figure from Letelier et al, (2019).

The study conducted by Ulloa and Letelier (2022) aimed to investigate energy transfer rates and mixing of thermally driven flows in Hele-Shaw cells. One notable finding was the establishment of a close relationship between the degree of mixing (χ), which characterizes the extent of temperature homogenization within the inner domain resulting from mixing, and an estimate of the thickness of the thermal boundary layer (Figure 2.10). This finding suggests the potential for parameterizing the degree of mixing based on the characteristics of the thermal boundary layer. *It is important to note that a constant Prandtl number of 7 was maintained throughout the study. However, it is widely acknowledged that the Prandtl number plays a critical role in determining the characteristics of the thermal boundary layer (TBL).*

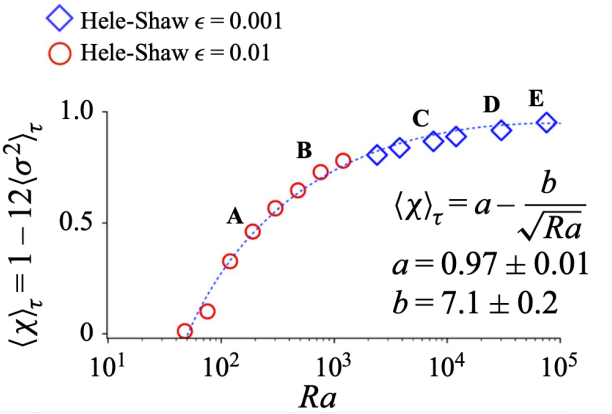

Figure 2.10: The degree of mixing, which represents the extent of temperature homogenization, was investigated as a function of the Rayleigh number in the Hele-Shaw numerical experiments. The degree of mixing was computed and a fitting approach was applied to establish the relationship between the two variables. Figure from Ulloa and Letelier (2022).

They also do a characterization of the dynamics, they conclude that megaplumes detach from the thermal boundary layer and occupy most of the domain, creating preferential pathways to transport fluid from top to bottom, homogenizing the temperature of the inner region and thus, increasing the degree of mixing of the system. They also observed that the megaplumes have an impact on the thermal boundary layers, reducing their size and forcing the emerging protoplumes to diverge laterally and merge with the megaplumes.

2.4. Scientific question

The literature review highlights several important questions that require further investigation. In the present work, we aim to address the following key questions:

1. To what extent can the HSM retain the physics of 3D convection in confined environments?

2. What is the effect of the Prandtl number on the heat transport dynamics in Hele Shaw cells?

2.5. Hypothesis

Based on the literature review and the articles by De Paoli et al. (2020) and Letelier et al. (2019), it is clear that the Hele-Shaw regime exists. However, there is a difference between the regime limit and the limit obtained by the presented mathematical model. Therefore, based on the articles and simulations by Letelier et al. (2019) and Ulloa and Letelier (2022), the validity of the Hele-Shaw model should be for $\epsilon^2 Ra = 0.05$.

Regarding the effect of the Prandtl number, it only appears in the inertial terms. Based on the articles by Letelier et al. (2019) and Ulloa and Letelier (2022), the main reason for the decrease in heat transport as the cell gap increases is dispersion. Moreover, as the Prandtl number increases, the HSM becomes more similar to a Darcy model. This is also observed

in simulations with free fluids in 3D, not only in confined environments (Chong et al., 2018) but also in unconfined environments (Ahlers et al., 2009). Taking this into account, it is possible to consider that the Prandtl number has an effect up to a certain value, and for values greater than this, it may no longer be significant.

2.6. Objectives

2.6.1. General objective

This thesis work has a clear objective to study and characterize the Hele-Shaw model (HSM), thoroughly examine their limits and scope, and investigate the behavior of the system under variations of the dimensionless numbers governing the problem, particularly the Prandtl number.

2.6.2. Specific objectives

In order to achieve the general objectives, there are three specific objectives:

- To determine the validity range of the Hele-Shaw cell model derived by Letelier et al. (2019), a comparison will be made with the results obtained by Chong and Xia (2016), which correspond to 3D simulations of free fluids in highly confined environments.
- Characterize the thermal boundary layer based on the dimensionless numbers Ra, Pr, and the cell anisotropy ϵ, by calculating the Nusselt number Nu and constructing scalings as functions of these dimensionless numbers, with a specific focus on the effect of the Prandtl number.

2.7. Expected results

The main outcome of this work is to validate the Hele-Shaw model (HSM) by comparing the results obtained from this 2D model with those from 3D literature. Furthermore, it aims to comprehend the influence of the Prandtl number in this set of equations, contributing to a deeper understanding of the fluid dynamics of this model.

2.8. Methodology

The framework considers a vertical Hele-Shaw cell in which an incompressible Boussinesq fluid is heated from below and cooled from the top. The dimensions of the cell in the y^*, x^* and z^* directions are denoted as b, L and H, respectively. The ratio b/H is small enough to treat the geometry as quasi-2D (Q2D), meaning that the flow is mainly confined to the cell plane (x-z). The density of the fluid, denoted as ρ^*, varies with temperature T^* according to the linear constitutive relation $(\rho^* - \rho_c)/\rho_c = \alpha(T^* - T_c)$, where $\rho^*(T_c) = \rho_c$ is the reference density at T_c and α is the thermal expansion coefficient of the fluid. We define the Boussinesq density component as $\tilde{\rho}^* = \rho^* - \rho_c$ and the modified pressure as $\tilde{p}^* = p^* + \rho_c g z^*$.

The momentum diffusivity (μ) and thermal diffusivity (κ) are assumed to be constant. The non-dimensional form of the dimensional variables $\{\boldsymbol{x}^*, t^*, \boldsymbol{v}^*, \tilde{p}^*, T^*, \tilde{\rho}^*\}$ is:

$$\boldsymbol{x} = \frac{\boldsymbol{x}^*}{H}\ ,\ t = \frac{t^*}{H/u_c}\ ,\ \boldsymbol{v} = \frac{\boldsymbol{v}^*}{u_c}\ ,\ p = \frac{\tilde{p}^*}{p_c}\ ,\ T = \frac{T^* - T_c}{\Delta T}\ ,\ \rho = \frac{\tilde{\rho}^*}{\alpha \Delta T} = -T\ , \tag{2.15}$$

With $\boldsymbol{x} = x\,\hat{x} + z\,\hat{z}$ the position, $\boldsymbol{v} = u\,\hat{x} + w\,\hat{z}$ the velocity field, $\Delta T = T_h - T_c > 0$ the temperature difference between the top (T_c) and bottom (T_h) boundaries of the cell, g the gravitational acceleration, $u_c = \alpha \Delta T g K/\mu$ the characteristic velocity and $p_c = \alpha \Delta T g H$ the characteristic pressure, where K is the permeability of the porous medium defined as $K = b^2/12$. Therefore, the nondimensional HSM (Letelier et al., 2019) – corrected up to $O(\epsilon^4)$ – is the following:

$$\partial_i v_i = 0\,, \tag{2.16a}$$

$$\frac{\partial T}{\partial t} + v_i\,\partial_i T = \frac{1}{Ra}\,\partial_i^2 T + \epsilon^2 Ra \left\{ \frac{2}{35}\ \partial_j \Big((v_i\,\partial_i T)\, v_j \Big) \right\}, \tag{2.16b}$$

$$v_i = -\partial_i p + T\,\delta_{iz} - \epsilon^2 \left\{ \frac{Ra}{Pr} \left(\frac{6}{5}\frac{\partial v_i}{\partial t} + \frac{54}{35}\, v_j\,\partial_j v_i \right) - \partial_j^2 v_i + \frac{2}{35} Ra\,(v_j\,\partial_j T)\,\delta_{iz} \right\}. \tag{2.16c}$$

These equations are the same as those presented in 2.12, 2.13 and 2.14; however, this way of writing them further highlights the analogy with a Darcy model incorporating inertial and dispersive terms proper to the cell geometry. The dimensionless numbers governing the problem are defined as follows:

$$Ra = \frac{\alpha \Delta T g K H}{\rho_c \kappa_c \nu_c} \tag{2.17}$$

$$Pr = \frac{\nu}{\kappa} \tag{2.18}$$

$$\epsilon = \frac{\sqrt{K}}{H} = \frac{b}{H\sqrt{12}} = \frac{\Gamma}{\sqrt{12}} \tag{2.19}$$

Global heat transport can be analyzed by using the Nusselt number, which is defined as follows (Letelier et al., 2019):

$$Nu = -\left.\frac{\partial \langle T \rangle_h}{\partial z}\right|_{z=0} \tag{2.20}$$

Where $<>_h$ denotes average in the horizontal direction. Another parameter of interest is the degree of mixing in the system (χ), which indicates how well-mixed the cell domain is. It takes a value of 0 if the system is completely stratified (in a conductive state) and 1 if the system is fully mixed. However, it is physically impossible for the degree of mixing to reach a value of 1 due to the presence of thermal boundary layers. The degree of mixing is calculated as follows (Ulloa & Letelier, 2022):

$$\chi = 1 - 12\sigma^2 \tag{2.21}$$

Where $\sigma = \langle T^2 \rangle_h - \langle T \rangle_h^2$. The last important parameter to be calculated in this study is

the thermal dissipation rate. The thermal dissipation rate is analogous to the widely studied scalar dissipation rate in fluid mixing and quantifies the level of irreversibility associated with heat transfer processes (Ulloa & Letelier, 2022). It is calculated as follows:

$$\vartheta = \frac{1}{Ra}(\partial_i T)^2 + \frac{2}{35}\epsilon^2 Ra(\partial_i(v_i T))^2 \tag{2.22}$$

However, the above expressions are time-dependent. To calculate a representative number, the temporal average $\langle Nu\rangle_\tau$, $\langle\chi\rangle_\tau$ and $\langle\vartheta\rangle_\tau$ will be computed using the formula 2.23 and 2.24. Figure 2.11 illustrates an example of statistically stable steady state Nusselt number.

$$\langle Nu\rangle_\tau = \frac{1}{T}\int_{\tau_0}^{\tau_0+T} Nu(t')dt'; \qquad \tau_0 >> 1 \tag{2.23}$$

$$\langle\chi\rangle_\tau = \frac{1}{T}\int_{\tau_0}^{\tau_0+T} \chi(t')dt'; \qquad \tau_0 >> 1 \tag{2.24}$$

$$\langle\vartheta\rangle_\tau = \frac{1}{T}\int_{\tau_0}^{\tau_0+T} \vartheta(t')dt'; \qquad \tau_0 >> 1 \tag{2.25}$$

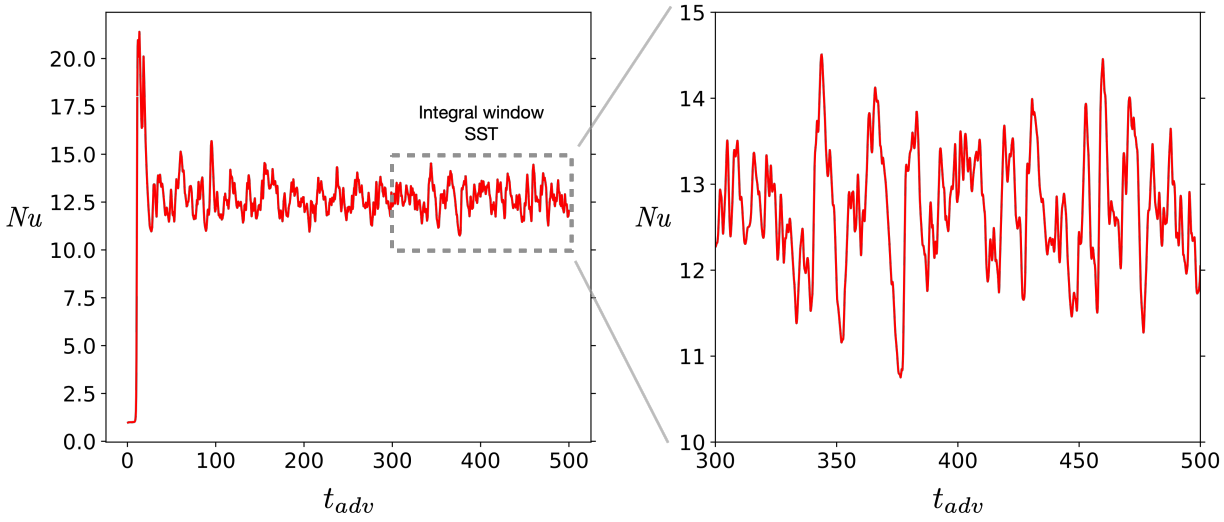

Figure 2.11: Nusselt vs advection time. An example of the Nusselt number calculation is shown in the time window where statistically steady behavior is observed. This simulation corresponds to $Pr = 30$, $\epsilon = 0.005$, and $Ra = 2000$, conducted in *Dedalus3* with no-slip boundary conditions in the z-direction and periodic boundary conditions in the x-direction.

The equations will be solved using two spectral solvers: *flow_solve* (Winters & de la Fuente, 2012) and *Dedalus* (Burns, Vasil, Oishi, Lecoanet, & Brown, 2020). These solvers will be employed to integrate the HSM equations 2.16 in both time and 2D space. The numerical methodology employed in this study involves two main approaches for discretization: trigonometric and Fourier expansions using *flow_solve*, and Fourier expansions and Chebyshev polynomials in *Dedalus*. The time step is carefully chosen to satisfy the Courant-Friedrichs-Lewy (CFL) condition, ensuring numerical stability and convergence. For all simulations, the CFL value remains below 0.01. The implementation of the *flow_solve* solver involves FORTRAN and MPI libraries for parallel computing. Within *flow_solve*, time inte-

gration is achieved using a third-order Adams-Bashforth scheme for advective and buoyant terms, complemented by the implicit fourth-order Adams-Moulton method for the diffusive scheme. In contrast, *Dedalus*, implemented in *Python3*, employs a 3rd-order 4-stage DIRK+ERK scheme and a 4th-order semi-implicit BDF scheme (Burns et al., 2020) for time integration. It is noteworthy that employing these different methods for time integration results in no significant changes in simulation time or alterations in the final results. This cross-validation ensures the reliability and accuracy of the numerical simulations throughout the study.

The lateral boundary conditions at $x = 0$ and $x = L'$ will be set as periodic, where L' represents the cell aspect ratio $L : H$. For the top and bottom boundaries, Dirichlet conditions will be imposed on the temperature, with $T(z = 0) = 1$ and $T(z = 1) = 0$. Regarding the velocity, two scenarios will be explored: free-slip and no-slip conditions (Fig. 2.12). Additionally, with free-slip boundary conditions, closed-box (CB) boundary conditions were also tested, which means that there is no penetration in the x-direction. All simulations will resolve the smallest physical scale of the problem, namely the Batchelor scale for $Pr > 1$ or the Kolmogorov scale for $Pr \leq 1$ (Gr˜tzbach & Karlsruhe, 1983). The analyses will be conducted after the quasi-steady state has been achieved.

To compare with the results of Chong and Xia (2016) , three different cell apertures will be used: $\Gamma = 1/16, 1/32$, and $1/64$. The Prandtl number will be kept fixed at 4.38, while the Rayleigh numbers will be varied in each case until the data deviate from the 3D simulations of Chong and Xia (2016). To explore the influence of the Prandtl number in the system, a fixed Rayleigh number will be chosen, and the Prandtl numbers will be varied in the range of $[0.1, 100]$.

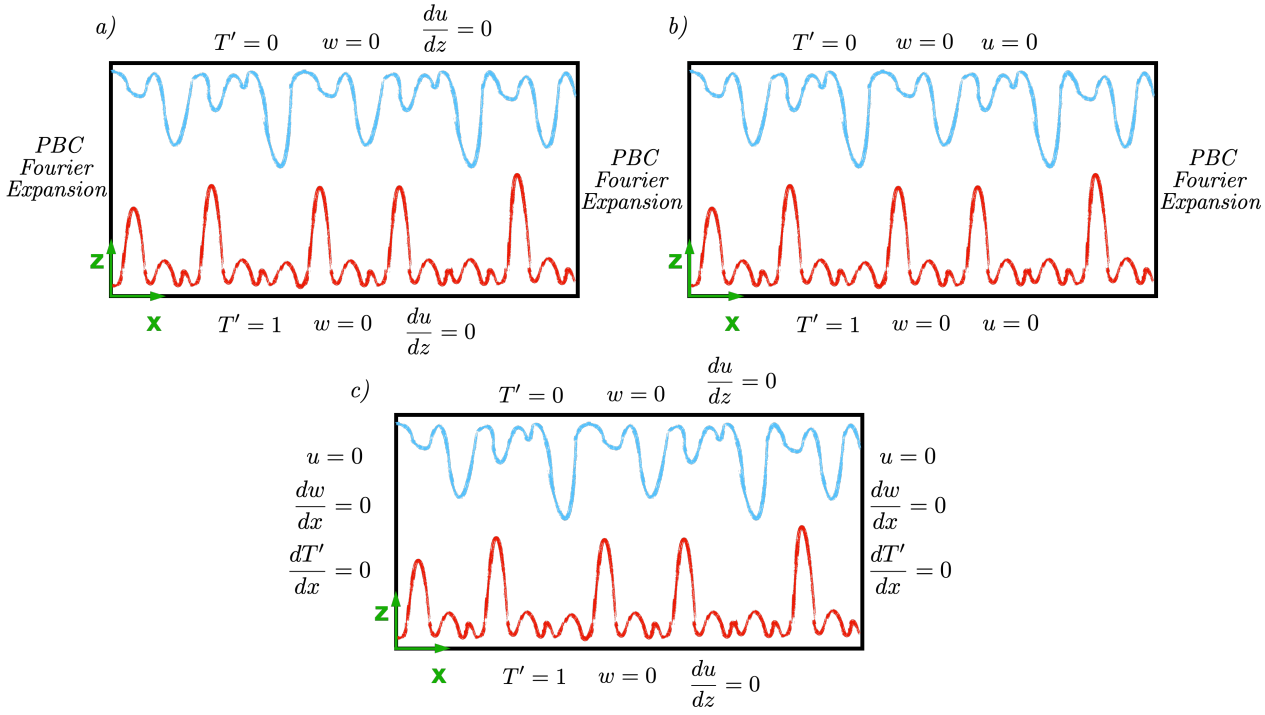

Figure 2.12: Difference between Boundary Conditions: a) Shows periodic boundary conditions (PBC) in the x-direction and free slip conditions in the z-direction. b) Shows periodic boundary conditions (PBC) in the x-direction and no-slip conditions in the z-direction. c) Shows closed-box boundary conditions (CB) in the x-direction with free slip conditions in the z-direction.

Chapter 3

Modeling heat transfer in severely confined environments

Below, we present the draft for the article titled "Modeling Heat Transfer in Severely Confined Environments", which is currently under preparation for submission to the journal *Physical Review Fluids*:

Modeling heat transfer in severely confined environments

Pablo Vergara and Juvenal A. Letelier*

Laboratory for Advanced studies of Geophysical and Subsurface Flows (g_3oLab) and Departamento de Ingeniería Civil, Universidad de Chile, Chile

Daisuke Noto and Hugo N. Ulloa

Department of Earth and Environmental Science, University of Pennsylvania, PA, USA

(Dated: July 30, 2023)

Abstract

The two-dimensional (2D) Hele-Shaw equations [1] has been recently introduced to model convection in severely confined environments. Yet, the system's parameters must still be bounded for sound application. In this paper, we assess the applicability of the Hele-Shaw model in accurately simulating thermal convection in severely confined three-dimensional (3D) systems. For this, we investigate the canonical problem of Rayleigh-Bénard convection in terms of the Rayleigh number, the Prandtl number, and the geometric aspect ratio of the fluid space. Here, we report the conditions under which the Hele-Shaw model successfully reproduces global quantifies of convection, encompassing the Darcian and Hele-Shaw regimes and the transition towards fully 3D environments. Our results provide insights into scenarios where the Hele-Shaw model reliably captures the essential convection features, providing a robust framework for investigating heat transfer in confined geometries and reconciling reported experimental data in Hele-Shaw cells.

Thermal convection, a fundamental phenomenon of the very fabric of nature, unfolds across myriad environments, each with distinctive degrees of confinement and spatiotemporal scales [2–6]. These environments range from unbounded 3D systems, such as the atmosphere, oceans, and lakes, where the horizontal scales of convective cells are much smaller than the environment's extent, to highly constrained porous and fractured media beneath the Earth's surface. Understanding convection in confined spaces is therefore crucial for characterizing natural and engineering systems [7–11].

Recently, the so-called Hele-Shaw model (HSM) [1] has been introduced to model and investigate the fluid dynamics of convection in environments where one dimension is greatly clenched [12–16]. Derived from the 3D Navier-Stokes equations (NSE) under the Boussinesq approximation, the HSM is a 2D set of equations for momentum and heat transfer that captures the macroscopic physics observed in permeable media flow while integrating perturbative corrections that quantify weak inertial and dispersive effects [17–19].

Thus, HSM is conceptualized as a mathematical bridge between the NSE and the Darcy equations (DE) for porous media in which inertia vanishes. Recent laboratory studies have validated numerical results obtained from the HSM [13, 14, 20], yet no study has constrained the magnitude of the perturbation parameters. This letter reports a numerical investigation that establishes the extent to which the HSM can be applied for modeling heat transfer in

* juvenal.letelier@uchile.cl

severely confined 3D environments.

In the case of porous and severely confined media, the relevant parameter controlling the fluid dynamics is the 'Rayleigh-Darcy number' $\mathrm{Ra} = \alpha \Delta T g K H / \nu \kappa$, being α the thermal expansion coefficient of the fluid, ΔT the temperature contrast, g the gravity acceleration, K the permeability, H the thickness of the porous layer, ν the momentum diffusivity and κ the thermal diffusivity [21]. For fluids with constant diffusivities, the coupling between the fine-to-large structures, and vice-versa, is notably linked by the elegant linear relation $\mathrm{Nu} \sim \mathrm{Ra}$ [22] valid for the ultimate regime, i.e. $\mathrm{Ra} \gtrsim 10^4$, with Nu the Nusselt—non-dimensional heat flux. On the other hand, Letelier *et al.* [1] proposed the HSM to study convection in Hele-Shaw cells heated from below and top (HS-RBC) that mimic, for instance, heat transport through fractures within the lithosphere [23**?**]. The perturbative corrections to the Darcy law included in the HSM are weighted by the ratio between the root square of the cell's permeability $K = b^2/12$ (function of the slot width b) and cell's height H, $\epsilon = \sqrt{K}/H$—the anisotropy ratio. Utilizing the HSM, Letelier *et al.* [1] reported sub-linear relations $\mathrm{Nu} \sim \mathrm{Ra}^{\gamma(\epsilon)}$, being $1/3 \leq \gamma(\epsilon) \leq 0.9$ for moderate Ra [24]. The authors showed the significant control that ϵ exerts on the net heat flux: the decrease of ϵ leads to the increase of γ and Nu. A sound construction of the above scaling law is relevant for modeling heat transfer in geothermal reservoirs, as standard Darcy models may not adequately resolve convection occurring through faults and fractured media [25–27].

A fundamental quest is characterizing the transition from quasi-2D (Q2D) to 3D convection. Chong and Xia [3] investigated the effect of cell confinement on heat transfer and flow topology by performing 3D numerical experiments that varied the domain geometry from fully 3D to a Q2D configuration. The authors adopted the 'standard Rayleigh number' $\mathrm{Ra}_f = \alpha \Delta T g H^3 / \nu \kappa$, the Prandtl number $\mathrm{Pr} = \nu/\kappa$ and the width-to-height aspect ratio $\Gamma = b/H = \sqrt{12}\,\epsilon$ to examine the system response. A remarkable finding was that the large convective cell observed in 3D RBC transformed into coherent wall-to-wall megaplumes for Γ small, analogue to the convective structures found in porous media convection [24, 28]. The last result leads us to the following question: *To what extent can the HSM retain the physics of 3D convection in confined environments?*

Through direct numerical simulations and comparison with the results by Chong and Xia [3], we demonstrate that the HSM resolves from porous media to 3D thermal convection dynamics in the 'Hele-Shaw regime' when "$\epsilon^2 \mathrm{Ra} \leq 0.1$". Additionally, utilizing the Rayleigh-

Darcy number, we show that (i) the onset of convection from Chong and Xia's data is $\mathrm{Ra}_c = 4\pi^2$ — the theoretical value predicted for porous media convection — and (ii) Nu increases dramatically as ϵ decreases.

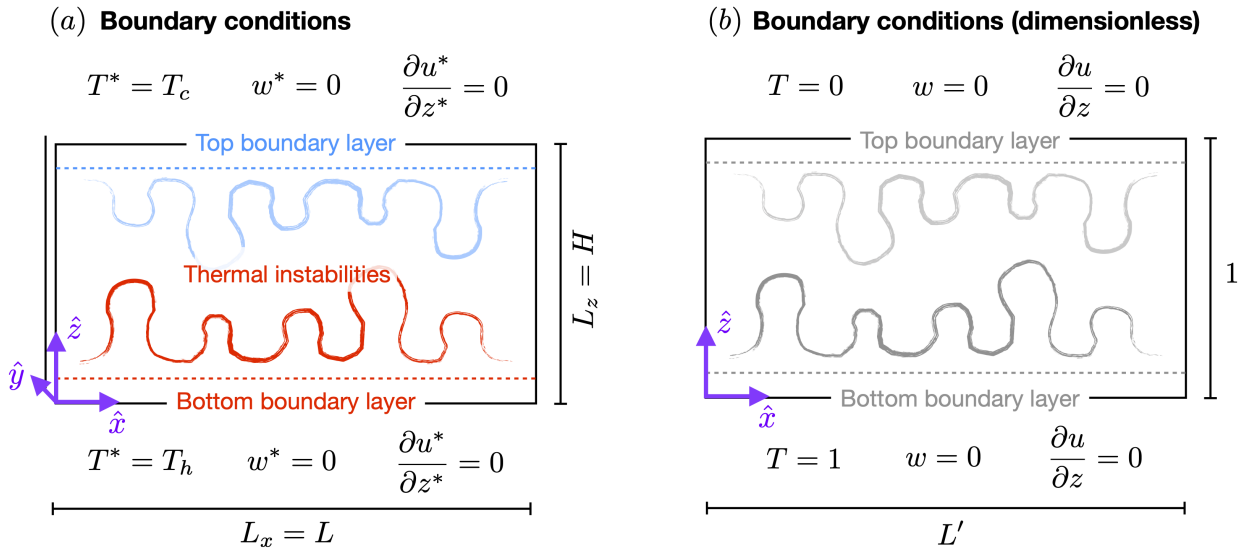

FIG. 1. Example of figure to continue writing. Nusselt number versus Rayleigh-Darcy number. (a) Numerical results of RBC by Chong and Xia [3] for a range of $\Gamma \in [1/128, 1/16]$ along with results by Hewitt *et al.* [24] for porous media convection. (b) Close-up for low-Nu and low-Ra; comparison between fully 3D numerical simulations and 2D HSM for $\Gamma = 1/16$.

Our framework considers an incompressible Boussinesq fluid within a vertical Hele-Shaw cell heated from below and cooled from top. The slot width, horizontal length and vertical height are b, L and H in the y^*, x^* and z^* directions, respectively. The ratio b/H is small enough to consider this geometry as Q2D, i.e., the flow is preferentially developed along the cell plane (x-z). The fluid density ρ^* varies with the temperature T^* following the linear constitutive relation $(\rho^* - \rho_c)/\rho_c = \alpha\,(T^* - T_c)$, with $\rho^*(T_c) = \rho_c$ a reference density and α the fluid thermal expansion coefficient. We define the Boussinesq density component as $\tilde{\rho}^* = \rho^* - \rho_c$ and the modified pressure as $\tilde{p}^* = p^* + \rho_c g z^*$. Momentum ($\mu$) and thermal ($\kappa$) diffusivities are assumed constant. The non-dimensional form of the dimensional variables $\{\boldsymbol{x}^*, t^*, \boldsymbol{v}^*, \tilde{p}^*, T^*, \tilde{\rho}^*\}$ is

$$\boldsymbol{x} = \frac{\boldsymbol{x}^*}{H}\ ,\ t = \frac{t^*}{H/u_c}\ ,\ \boldsymbol{v} = \frac{\boldsymbol{v}^*}{u_c}\ ,\ p = \frac{\tilde{p}^*}{p_c}\ ,\ T = \frac{T^* - T_c}{\Delta T}\ ,\ \rho = \frac{\tilde{\rho}^*}{\alpha \Delta T} = -T\ , \tag{1}$$

with $\boldsymbol{x} = x\,\hat{x} + z\,\hat{z}$ the position, $\boldsymbol{v} = u\,\hat{x} + w\,\hat{z}$ the velocity field, $\Delta T = T_h - T_c > 0$ the

temperature difference between the top (T_c) and bottom (T_h) boundaries of the cell, g the gravitational acceleration, $u_c = \alpha \Delta T g K/\mu$ the characteristic velocity and $p_c = \alpha \Delta T g H$ the characteristic pressure. Therefore, the nondimensional HSM [1] – corrected up to $O(\epsilon^4)$ – is the following:

$$\partial_i v_i = 0\,, \tag{2a}$$

$$\frac{\partial T}{\partial t} + v_i\,\partial_i T = \frac{1}{\mathrm{Ra}}\,\partial_i^2 T + \epsilon^2 \left\{ \frac{2}{35}\,\mathrm{Ra}\,\partial_j\big((v_i\,\partial_i T)\,v_j\big) \right\}, \tag{2b}$$

$$v_i = -\partial_i p + T\,\delta_{iz} - \epsilon^2 \left\{ \frac{\mathrm{Ra}}{\mathrm{Pr}} \left(\frac{6}{5}\,\frac{\partial v_i}{\partial t} + \frac{54}{35}\,v_j\,\partial_j v_i \right) - \partial_j^2 v_i + \frac{2}{35}\mathrm{Ra}\,(v_j\,\partial_j T)\,\delta_{iz} \right\}. \tag{2c}$$

The model (2) results from averaging the NSE and the advection-diffusion model for heat transport in the spanwise $\hat{y}$ direction, integrating no-slip and no-flux boundary conditions at the vertical walls [1]. The latter can be considered as a correction of the advection-diffusion model for heat transfer (2b) and Darcy equation (2c), incorporating inertial and dispersive terms proper to the cell geometry.

We employ the spectral solvers *flow_solve* [29] and *Dedalus* [30] to integrate the HSM (2) in time and the 2D space. The lateral boundary conditions at $x = 0$ and $x = L'$ are periodic, with $L' = L/H$ the cell aspect ratio. On the top and bottom boundaries, we impose Dirichlet conditions for the temperature, $T(z = 0) = 1$ and $T(z = 1) = 0$, whereas for the velocity, we explore two scenarios for velocity, free-slip and no-slip conditions (see schematic in Fig. 1). The free-slip scenarios were run using *flow_solve*; these numerical experiments are analogue to those in [31], so we refer the reader to [31] for detailed information about the numerical implementation. In contrast, no-slip scenarios were run using *Dedalus*.

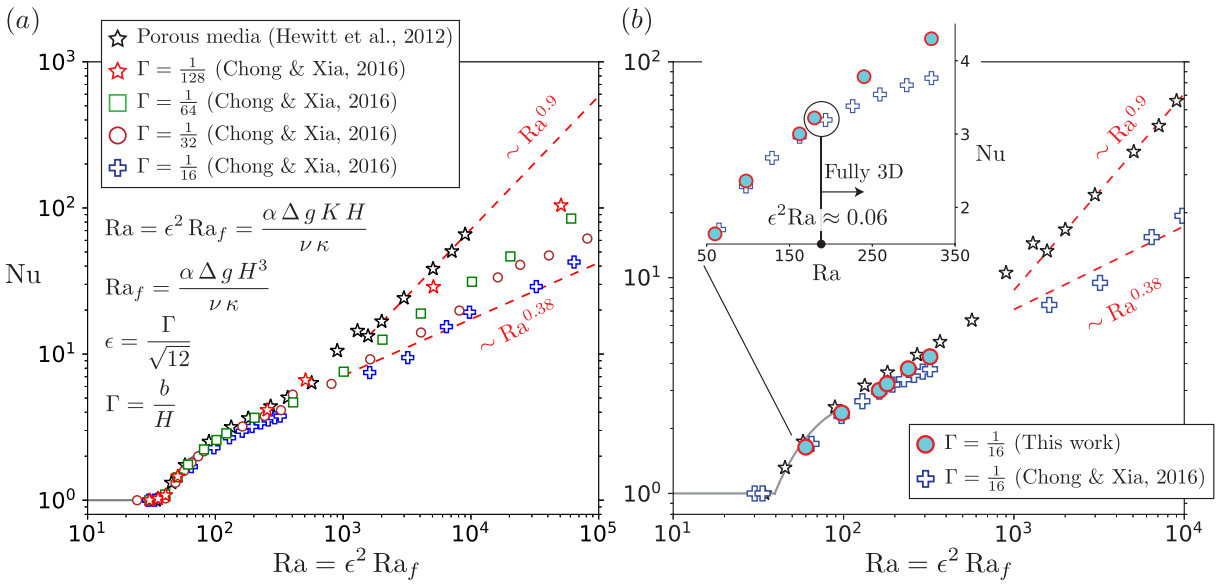

FIG. 2. Nusselt number versus Rayleigh-Darcy number. (a) Numerical results of RBC by Chong and Xia [3] for a range of $\Gamma \in [1/128, 1/16]$ along with results by Hewitt *et al.* [24] for porous media convection. (b) Close-up for low-Nu and low-Ra; comparison between fully 3D numerical simulations and 2D HSM for $\Gamma = 1/16$. The upper red dashed line shows the fitting curve for porous media results by Hewitt *et al.* [24] ($\mathrm{Nu} \sim \mathrm{Ra}^{0.9}$). The lower red dashed line shows the fitting curve for 3D results with $\Gamma = 1/16$ and $\mathrm{Ra} > 10^3$ by Chong and Xia [3]

Fig. 2a presents a mapping of the 3D numerical simulations conducted by Chong and Xia [3] in terms of the Nusselt number (Nu) and the Rayleigh-Darcy number, expressed as $\mathrm{Ra} = \epsilon^2 \mathrm{Ra}_f$, where the anisotropy ratio and the standard Rayleigh number are considered. Detailed information on the computation of Nu can be found in Chong and Xia [3]. On the other hand, for the HSM, we calculate the Nusselt number as $\mathrm{Nu} = \frac{\partial \langle T \rangle_h}{\partial z}\Big|_{z=0}$ utilizing the dimensionless horizontal average $\langle f \rangle_h = (1/L') \int_0^{L'} f \, \mathrm{d}x$. The dataset includes various aspect ratios ($\Gamma = \sqrt{12}\,\epsilon$) representing a range of confinements, from low confinement ($\Gamma = 1/16$) to high confinement ($\Gamma = 1/128$). The results demonstrate that regardless of the aspect ratio Γ, the data collapse when Ra approaches $4\pi^2$, the critical value for the onset of convection in porous media —the Darcian regime [1]. Depending on the degree of confinement, for intermediate Rayleigh values ($10^2 < \mathrm{Ra} < 10^3$) the data shows deviations from the curve obtained for porous media, a regime associated to weak contributions from $\hat{y}$ direction (confinement) in heat transfer —the Hele-Shaw regime [1]. However, for higher Rayleigh

numbers ($\mathrm{Ra} > 10^3$), the trajectories of the curves diverge significantly from each other. One of the notable effects of varying the degree of confinement is observed in the power law relationship between Nu and Ra. In the limit cases of porous media [22] or extreme confinement [1], heat efficiently transfers from wall-to-wall following the scaling law $\mathrm{Nu} \sim \mathrm{Ra}^{0.9}$ [24]. As the system becomes more three-dimensional, i.e., with larger values of Γ, the exponent of the scaling law converges towards its theoretical value of 1/3 for intermediate values of the classic Rayleigh number [32] or high-Ra scenarios [3, 31]. On the other hand, Fig. 2*b* presents numerical results of the HSM (shown as circles) for $\Gamma = 1/16$ and utilizing no-slip boundary conditions for the bottom and top walls, demonstrating its performance in comparison to fully 3D results [3] and porous media data [24]. We observe that the HSM accurately represents the fully 3D outcomes when the Rayleigh number (Ra) is low. However, as the Ra value increases, a noticeable discrepancy emerges between the two models. The inset of Fig. 2*b* provides further insight, revealing that the HSM begins to overestimate the heat transfer rate relative to the 3D results for $\Gamma^2\mathrm{Ra} \sim 0.7$ or $\epsilon^2\mathrm{Ra} \sim 0.06$. The latter represents a conservative estimation of the validity of the HSM for $\Gamma = 1/16$, recovering Chong and Xia' data [3] when $\mathrm{Ra} \lesssim 180$.

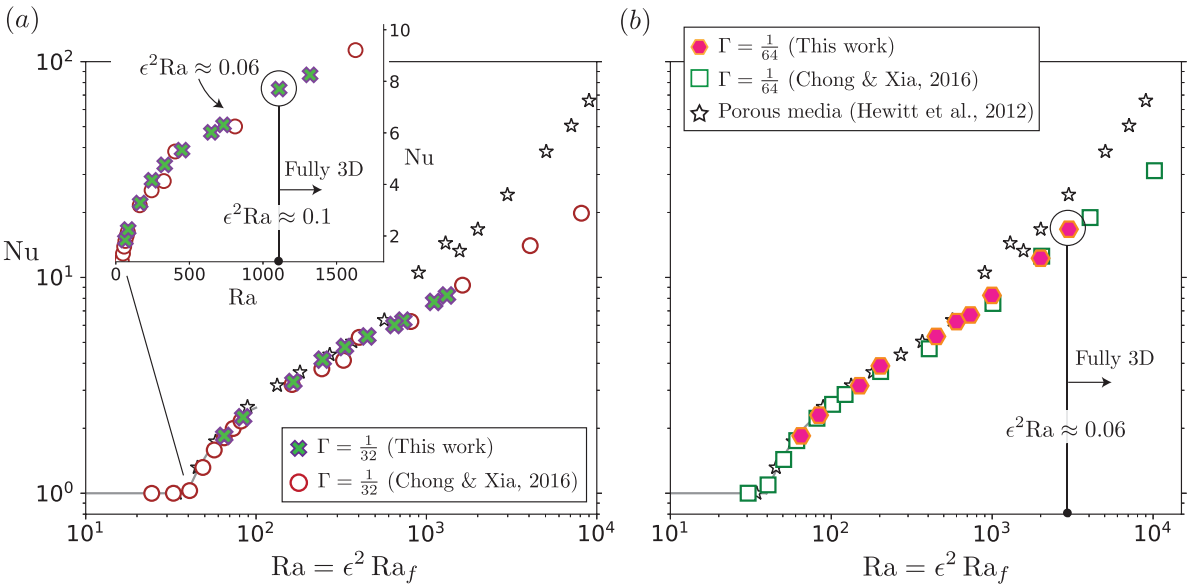

FIG. 3. Nusselt Number versus Rayleigh-Darcy Number. Panels (*a*) and (*b*) show comparative analysis of Chong and Xia [3] 3D simulations and HSM results for $\Gamma = 1/32$ and 1/64, respectively. Data by Hewitt *et al.* [24] is displayed in stars.

Fig. 3 illustrates the relationship between the Nusselt number and the Rayleigh-Darcy number for two different geometrical aspect ratios, $\Gamma = 1/32$ and $\Gamma = 1/64$. Similar to Figure 2, it displays the 3D numerical results by Chong and Xia [3], the results obtained from the Darcy model [24], and our findings using the HSM. The curves generated by these models exhibit complete overlap within the range of $\mathrm{Ra}_c \leq \mathrm{Ra} < 500$. However, for larger values of Ra, the Darcy model results deviate from the trend observed in the 3D NSE and the HSM, which remain in agreement until approximately $\mathrm{Ra} \sim O(10^3)$. In the inset of Fig. 3(a), we observe that the divergence between the HSM and the 3D NSE occurs within the range of $0.06 \leq \epsilon^2\mathrm{Ra} \leq 0.1$. This threshold for $\epsilon^2\mathrm{Ra}$ is also evident in environments with $\Gamma = 1/64$, as demonstrated in Fig. 3(b).

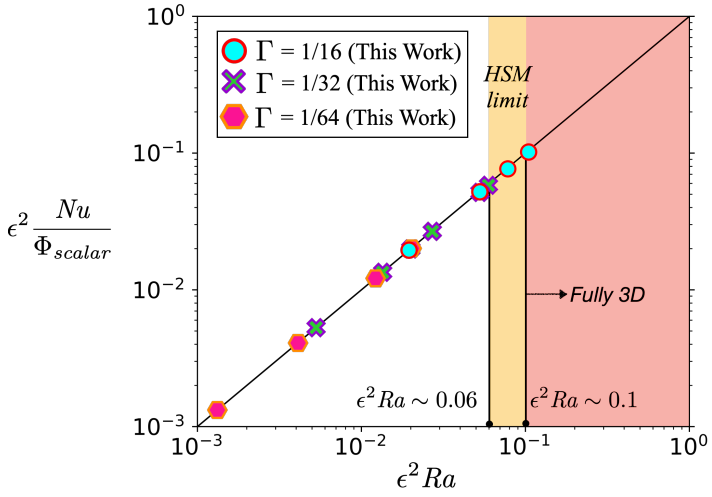

FIG. 4. Collapsing data in a universal curve. $\epsilon^2\mathrm{Nu}/\Phi_{scalar}$ as a function of $\epsilon^2\mathrm{Ra}$. Shaded areas highlight the different dynamic regimes.

Letelier *et al.* [1] found a theoretical relationship between the Nusselt number (Nu), which characterizes convective heat transfer, and the rate of destruction of thermal fluctuations, denoted as Φ_{scalar}, associated with irreversible thermal mixing [31]. They discovered that $\mathrm{Nu} = \mathrm{Ra}\,\Phi_{scalar}$. The latter expression generalizes the results obtained by Otero *et al.* [33] and Hewitt *et al.* [24], for porous media, allowing a characterization of heat transfer rate in 3D severely confined environments. In Fig. 4, we present the behavior of $\epsilon^2\mathrm{Nu}/\Phi_{scalar}$ with respect to $\epsilon^2\mathrm{Ra}$, the fundamental quantity that determines the ability of the Hele-Shaw model (HSM) to capture the dynamics of thermal convection in confined geometries. Re-

markably, we reobtain the same linear power-law relationship predicted by theory [1]. This canonical relationship is not exclusive to thermal convection but has also been discovered in the problem of solutal convection [34–39], in the context of CO_2-brine mixing in highly confined environments [16]. For the analogue problem of CO_2-brine mixing, the ratio between the boundary mass flux (represented by the Sherwood number, Sh) and the rate of mixing between the dissolved carbon dioxide and brine (denoted as Φ_{scalar}) also follows a linear power law with Ra. We propose that the ratio $\mathrm{Nu}/\Phi_{scalar}$ serves as a fundamental quantity that enables a deeper understanding of the underlying physics of thermal convection through a wide range of confinement degrees. While we acknowledge the challenges in quantifying Φ_{scalar} through laboratory experiments, establishing a sound characterization of the relationship $\mathrm{Nu} \sim \mathrm{Ra}^{\gamma(\epsilon)}$ via numerical and laboratory experiments [3, 15] across various environments would allow us to infer the rate of mixing driven by convection in the bulk $\Phi_{scalar} \sim \mathrm{Ra}^{\gamma(\epsilon)-1}$. This knowledge would have practical applications in natural and engineering science, such as in geothermal and petroleum reservoir engineering [27, 40–43] and carbon dioxide sequestration [44–46].

Our findings suggest that the parameter $\epsilon^2\mathrm{Ra}$ exhibits a range of values rather than a single value to determine the upper limit of validity for the Hele-Shaw Model (HSM). Specifically, we demonstrate that the HSM accurately captures the overall characteristics of the fully 3D results within the range of $\epsilon^2\mathrm{Ra}$ values approximately between 0.06 and 0.1. This empirical observation establishes an upper threshold for the nondimensional quantity $\epsilon^2\mathrm{Ra}$ when investigating heat transfer rates in 3D confined environments using the HSM. By identifying this threshold, we provide a practical guide to utilize the HSM as a reliable modeling framework in the study of thermal convection in severely confined environments.

ACKNOWLEDGMENTS

[1] J. A. Letelier, N. Mujica, and J. H. Ortega, Journal of Fluid Mechanics **864**, 746 (2019).

[2] K. L. Chong, S.-D. Huang, M. Kaczorowski, K.-Q. Xia, *et al.*, Physical review letters **115**, 264503 (2015).

[3] K. L. Chong and K.-Q. Xia, Journal of Fluid Mechanics **805**, R4 (2016).

[4] K. L. Chong, S. Wagner, M. Kaczorowski, O. Shishkina, and K.-Q. Xia, Physical Review Fluids **3**, 013501 (2018).

[5] X.-J. Huang, Y.-P. Hu, and Y.-R. Li, Physics of Fluids **31**, 075107 (2019).

[6] O. Shishkina, Physical Review Fluids **6**, 090502 (2021).

[7] P. Kruger, Annual Review of Energy **1**, 159 (1976).

[8] R. N. Anderson, M. A. Hobart, and M. G. Langseth, Science **204**, 828 (1979).

[9] I. G. Donaldson, Annual Review of Earth and Planetary Sciences **10**, 377 (1982).

[10] L. Aresti, P. Christodoulides, and G. Florides, Renewable and Sustainable Energy Reviews **92**, 757 (2018).

[11] X. Bu, K. Jiang, H. Li, F. Ma, and L. Wang, Geothermal Energy **11**, 1 (2023).

[12] J. A. Letelier, P. Herrera, N. Mujica, and J. H. Ortega, Experiments in Fluids **57**, 1 (2016).

[13] M. De Paoli, M. Alipour, and A. Soldati, Journal of Fluid Mechanics **892**, 10.1017/jfm.2020.229 (2020).

[14] M. Alipour, M. De Paoli, and A. Soldati, Experiments in Fluids **61**, 1 (2020).

[15] D. Noto, H. N. Ulloa, and J. A. Letelier, Experiments in Fluids **64**, 74 (2023).

[16] J. Letelier, H. Ulloa, J. Leyrer, and J. Ortega, Journal of Fluid Mechanics **962**, A8 (2023).

[17] C. Ruyer-Quil, Comptes Rendus de l'Académie des Sciences-Series IIB-Mechanics **329**, 337 (2001).

[18] O. Kvernvold and P. A. Tyvand, Int. J. Heat Mass Transfer **24**, 887 (1981).

[19] C. Oltean, C. Felder, M. Panfilov, and M. Buès, Transport in porous media **55**, 339 (2004).

[20] D. Noto, H. N. Ulloa, and J. A. Letelier, in *75th Annual Meeting of the Division of Fluid Dynamics* (Bulletin of the American Physical Society, 2022).

[21] D. Nield and A. Bejan, *Convection in Porous Media*, 3rd ed. (Springer-Verlag New York, 2006) Chap. 6, pp. 212–221.

[22] C. R. Doering and P. Constantin, Journal of Fluid Mechechanics **376**, 263–296 (1998).

[23] J. A. Letelier, J. O'Sullivan, M. Reich, E. Veloso, P. Sánchez-Alfaro, D. Aravena, M. Muñoz, and D. Morata, Geothermics **89**, 101940 (2021).

[24] D. R. Hewitt, J. A. Neufeld, and J. R. Lister, Physical Review Letters **108**, 224503 (2012).

[25] Y. Cherubini, M. Cacace, G. Blöcher, and M. Scheck-Wenderoth, Environmental earth sciences **70**, 3603 (2013).

[26] J. W. Patterson, T. Driesner, S. Matthai, and R. Tomlinson, Journal of Geophysical Research:

Solid Earth **123**, 2658 (2018).

[27] G. Yan, B. Busch, R. Egert, M. Esmaeilpour, K. Stricker, and T. Kohl, EGUsphere **2022**, 1 (2022).

[28] S. Pirozzoli, M. De Paoli, F. Zonta, and A. Soldati, Journal of Fluid Mechanics **911**, 10.1017/jfm.2020.1178 (2021).

[29] K. B. Winters and A. de la Fuente, Ocean Model. **49-50**, 47 (2012).

[30] K. J. Burns, G. M. Vasil, J. S. Oishi, D. Lecoanet, and B. P. Brown, Physical Review Research **2**, 023068 (2020).

[31] H. N. Ulloa and J. A. Letelier, Journal of Fluid Mechanics **930**, 10.1017/jfm.2021.897 (2022).

[32] G. Ahlers, S. Grossmann, and D. Lohse, Rev. Mod. Phys. **81**, 503 (2009).

[33] J. Otero, L. A. Dontcheva, H. Johnston, R. A. Worthing, A. Kurganov, G. Petrova, and C. R. Doering, Journal of Fluid Mechanics **500**, 263–281 (2004).

[34] J. A. Neufeld, M. A. Hesse, A. Riaz, M. A. Hallworth, H. A. Tchelepi, and H. E. Huppert, Geophysical research letters **37**, 10.1029/2010GL044728 (2010).

[35] S. Backhaus, K.Turitsyn, and R. E. Ecke, Physical Review Letter **106**, 104501 (2011).

[36] J. J. Hidalgo, J. Fe, L. Cueto-Felgueroso, and R. Juanes, Physical Review Letter **109**, 10.1103/PhysRevLett.109.264503 (2012).

[37] D. R. Hewitt, J. A. Neufeld, and J. R. Lister, Journal of Fluid Mechanics **719**, 551 (2013).

[38] M. De Paoli, Phys. Fluids **33**, 016602 (2021).

[39] M. De Paoli, D. Perissutti, C. Marchioli, and A. Soldati, Phys. Rev. Fluids **7**, 093503 (2022).

[40] M. A. Grant and P. F. Bixley, *Geothermal Reservoir Engineering* (Elsevier, 2011) pp. 1–8.

[41] M. H. Dickson and M. Fanelli, *Geothermal energy: utilization and technology*, edited by M. Dickson (Routledge; 1st edition, 2013).

[42] S. Ghoreishi-Madiseh, F. Hassani, A. Mohammadian, and P. Radziszewski, Journal of Renewable and Sustainable Energy **5**, 043104 (2013).

[43] A. O. Gbadamosi, R. Junin, M. A. Manan, A. Agi, and A. S. Yusuff, International Nano Letters **9**, 171 (2019).

[44] B. Metz, O. Davidson, H. C. de Coninck, M. Loos, and L. A. Meyer, eds., *IPCC Special Report on Carbon Dioxide Capture and Storage. Prepared by Working Group III of the Intergubernamental Panel on Climate Change* (Cambridge University Press, Cambridge, United Kingdom and New York, NY, USA, 2005).

[45] S. M. Benson and D. R. Cole, Elements **4**, 325 (2008).

[46] F. Javadpour and J.-P. Nicot, Transp. Porous Media **89**, 265 (2011).

Chapter 4

Results

The following section presents a compilation of other results obtained in this study, some of which served as an initial starting point for the results published in the paper, while others explore different aspects of the Hele-Shaw regime. This chapter is divided into two subsections according to the temporal development of the work. There is a subsection presenting the results with free-slip boundary conditions, while another subsection focuses on the results with no-slip boundary conditions. In the latter subsection, a comparison between the results of both boundary conditions is also provided.

4.1. Exploring Hele Shaw Regime

4.1.1. Free Slip Simulations

In Figure 4.1, the temperature field resulting from the numerical simulations can be observed. It is clear that as the Rayleigh number increases, there is greater chaos in the system, transitioning from a stable system to a more chaotic one, a phenomenon observed in both porous media (Otero et al., 2004; Hewitt et al., 2012) and Hele-Shaw cells (Letelier et al., 2019). Additionally, there is little qualitative difference when changing the Prandtl number of the system. Although a difference can be observed between subplot b) and d), this can be attributed to the findings described by Bhattacharya et al. (2021), where higher Prandtl numbers result in increased flow inhomogeneity and higher fluctuations. It is also possible that the transition between the low and high Rayleigh regime is influenced by the Prandtl number. However, in terms of heat transport (Fig 4.3), the results are practically the same.

Figure 4.2 shows the temperature field and scalar dissipation rate for different Prandtl numbers. While there is no clear difference between the subplots for $Pr = 7$ and $Pr = 100$, the case with $Pr = 0.5$ exhibits distinctive features. Firstly, the temperature field appears to be more organized, with thicker and more coherent plumes, as also observed by Bhattacharya et al. (2021) in 2D free-flowing fluids as Prandtl number decreases. The scalar dissipation rate map also shows slight variations, likely influenced by the aforementioned effects. This difference is reflected in the Nusselt number of this simulation (Fig 4.5).

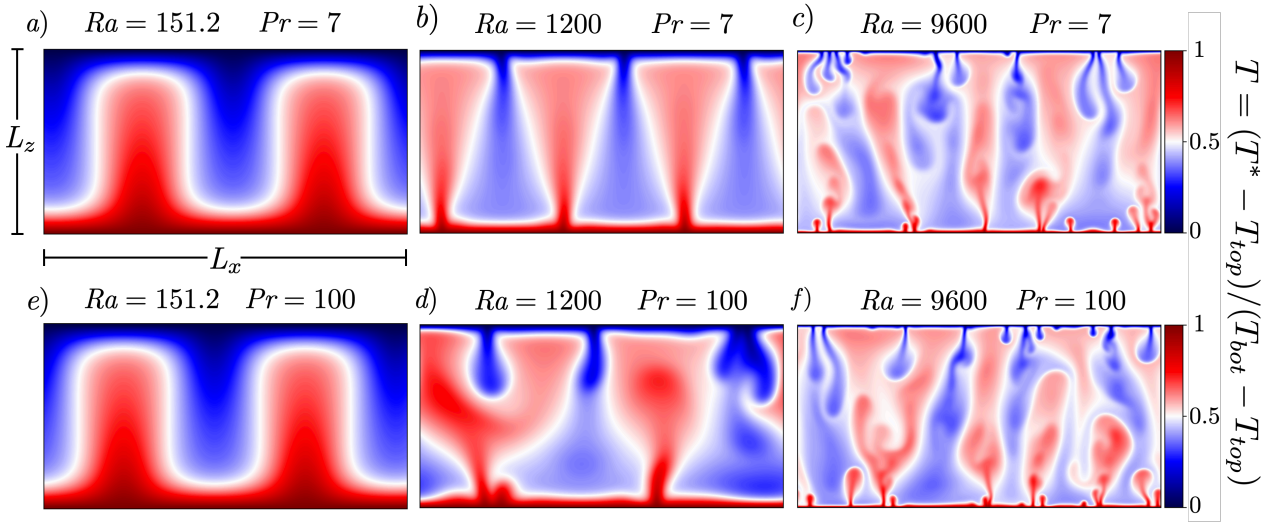

Figure 4.1: Numerical simulation results with $\epsilon = 5 \times 10^{-3}$, for two Pr values and three Ra values. (a-c) show the temperature field for Pr =7 and (e-f) for Pr =100. It can be seen that there are no major differences in the snapshots between the two Prandtl numbers presented.

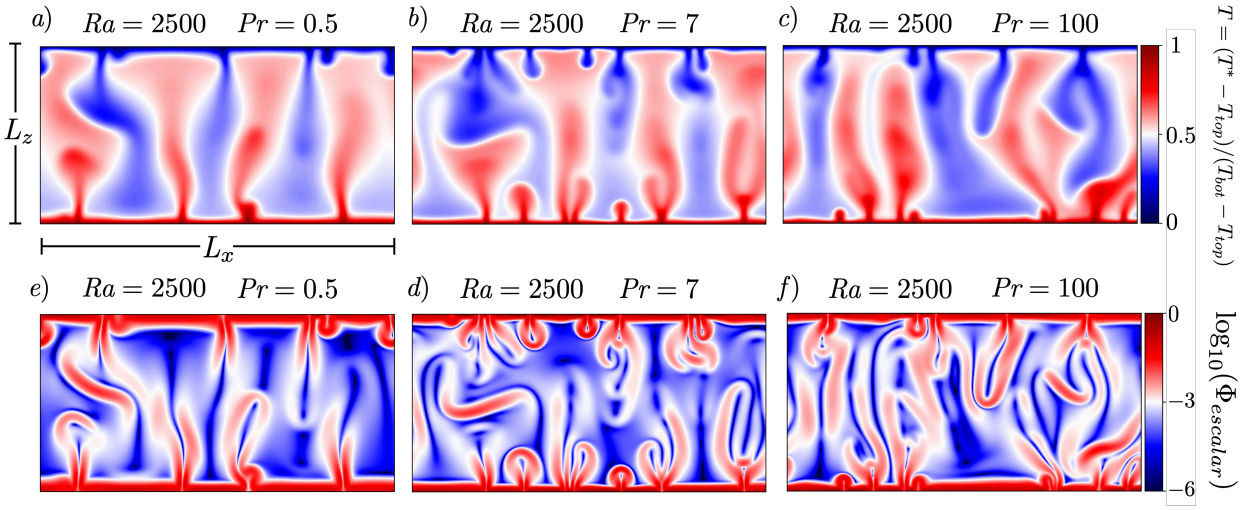

Figure 4.2: Numerical simulation results with $\epsilon = 5 \times 10^{-3}$, for three Pr values and one Ra value. (a-c) show the temperature field and (e-f) show the scalar dissipation field.

One of the most important results is shown in Figure 4.3. It can be observed that for the three plotted Prandtl numbers, namely $Pr = 7$, $Pr = 30$ and $Pr = 100$, the heat transport appears to be unaffected, yielding identical results until very high Rayleigh numbers (~ 6000), where the series for $Pr = 7$ starts to deviate slightly. As mentioned in the literature review, in this model, the only term containing the Prandtl number is the inertial correction, which scales with $\epsilon^2 Ra/Pr$. Therefore, both the invariance of the results and this detachment can be explained based on this term. As the Prandtl number increases, the inertial component becomes less important, resembling more and more a Darcy model where the Prandtl number either does not exist or is infinite. However, when this factor is sufficiently large, the inertial terms begin to contribute, as is the case when $\epsilon^2 Ra/Pr \sim 0.02$. This limit is merely an

estimate that can serve as an initial stepping stone to explore the behavior of inertial effects in the HSM. The characteristic change in slope between the Darcy regime and the Hele-Shaw regime (Letelier et al., 2019; De Paoli et al., 2020) is also observed, in this case the scaling law for $\epsilon = 0.005$ is $Nu \sim Ra^{0.85}$.

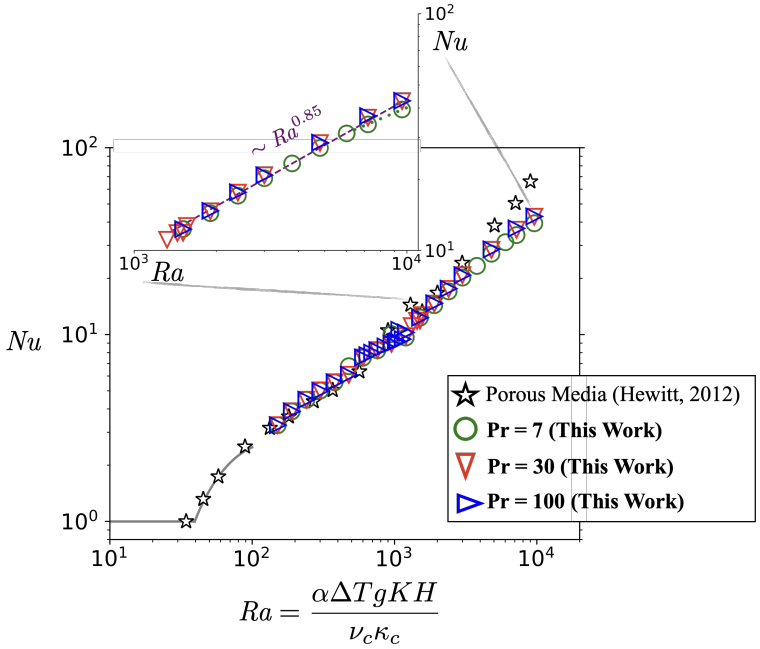

Figure 4.3: $\langle Nu \rangle_\tau$ as function of Ra for $\epsilon = 5 \times 10^{-3}$. It can be observed that for the simulated range, the dimensionless heat transport variation does not respond to Prandtl number variations in range $Pr \in [7, 100]$. In addition, the results obtained by Hewitt et al. (2012) for the porous medium model are plotted, where the deviation from the Darcy regime studied by Letelier et al. 2019 is observed. The insert shows the High-Rayleigh regime plot. The scaling law of all data in the high Rayleigh regime is $Nu \sim Ra^{0.65}$. In the Pr=7 simulation, the values with higher Rayleigh begin to detach from the others, presumably due to inertial effects.

Figure 4.4 shows the degree of mixing of the system as a function of the Rayleigh number. Similar to the Nusselt number, the system is not affected by changes in the Prandtl number within the range of $Pr \in [7, 100]$. This suggests that the thermal boundary layers are similar, as both the Nusselt number (Fig 4.3) and the degree of mixing do not respond, since the degree of mixing should ideally respond to changes in the thickness of the thermal boundary layer. This is consistent with the estimation that the thermal boundary layer is approximately inversely proportional to the Nusselt number (Grossmann & Lohse, 2000; Ahlers et al., 2009; King et al., 2013). Additionally, it is observed that higher Rayleigh numbers correspond to greater mixing in the system, which aligns with the findings of Ulloa and Letelier (2022). Also, a similar scaling law for the degree of mixing is obtained, showed in the Figure 4.4.

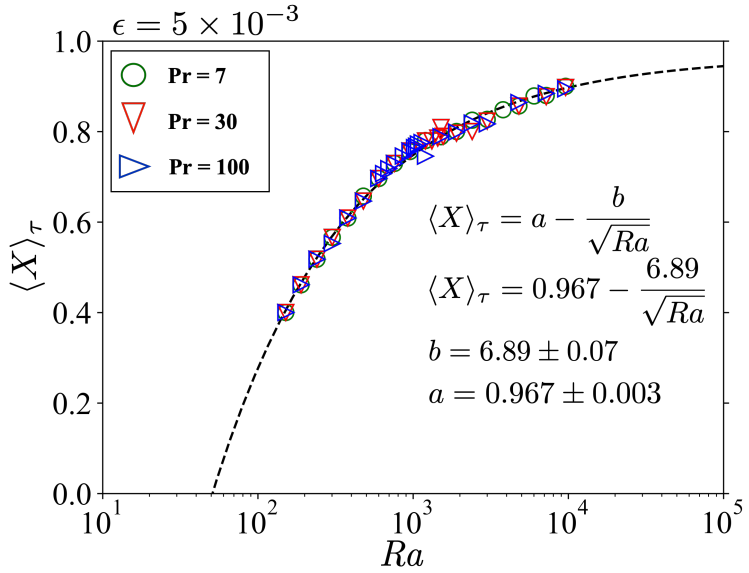

Figure 4.4: Degree of mixing of the system as a function of Rayleigh number. Like the Nusselt number, the value of this indicator does not respond to variations of the Prandtl number in the range Pr ∈ [7,100].

Only one Prandtl number below 1 was simulated, as shown in Figure 4.5. It is observed that there is indeed a decrease in heat transport, which is consistent with reductions reported in highly confined 3D free fluids (Chong et al., 2018). Although the results are not directly comparable due to differences in boundary conditions, there is a clear trend that under a certain Prandtl number, it starts to become important, decreasing heat transport. This trend is also observed in unconfined 3D free fluids (Ahlers et al., 2009). This suggests that for low Prandtl numbers, approximately $Pr < 1$, inertial effects start to impact the heat transport dynamics in the cell, reducing the effectiveness of heat transport. However, as mentioned earlier, it is better to take into account the effect of $\epsilon^2 Ra/Pr$. In this case $\epsilon^2 Ra/Pr \sim 0.12$, which falls outside the limit found in Figure 4.3.

Figure 4.6 displays the profiles of average temperature in the statistically steady state for $\epsilon = 0.005$. It can be seen that as the Rayleigh number increases, the core of the cell exhibits a more homogeneous temperature distribution, as observed in the degree of mixing (Fig 4.4). Additionally, differences in these profiles can be observed when varying the Prandtl number, with a slight distinction between the profile for $Pr = 0.5$ and the profiles for $Pr = 7$ and $Pr = 100$. This confirms the notion that the thermal boundary layer remains practically invariant within the range of $Pr \in [7, 100]$. However, for lower Prandtl numbers, the thermal boundary layer begins to thicken, creating greater resistance to heat transport and consequently lowering the Nusselt number.

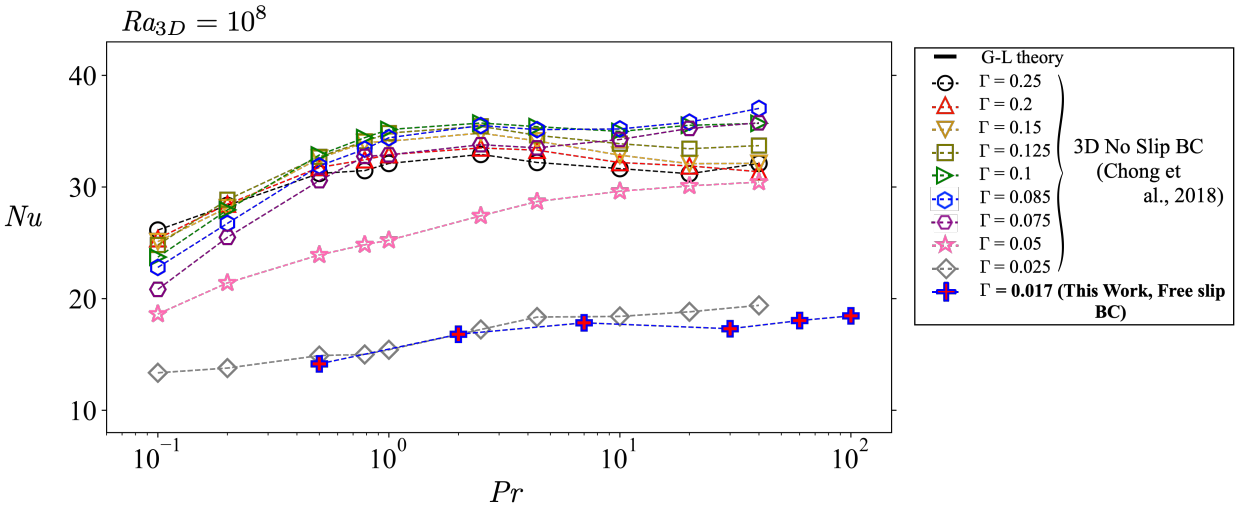

Figure 4.5: Nusselt number as a function of the Prandtl number for $\epsilon = 0.005$. Comparison between the results obtained in 3D free fluids by Chong et al. (2018) with no-slip boundary conditions. Although the boundary conditions are different and the results are not directly comparable, the decrease in Nusselt number for the simulation with $Pr = 0.5$ occurs in both cases.

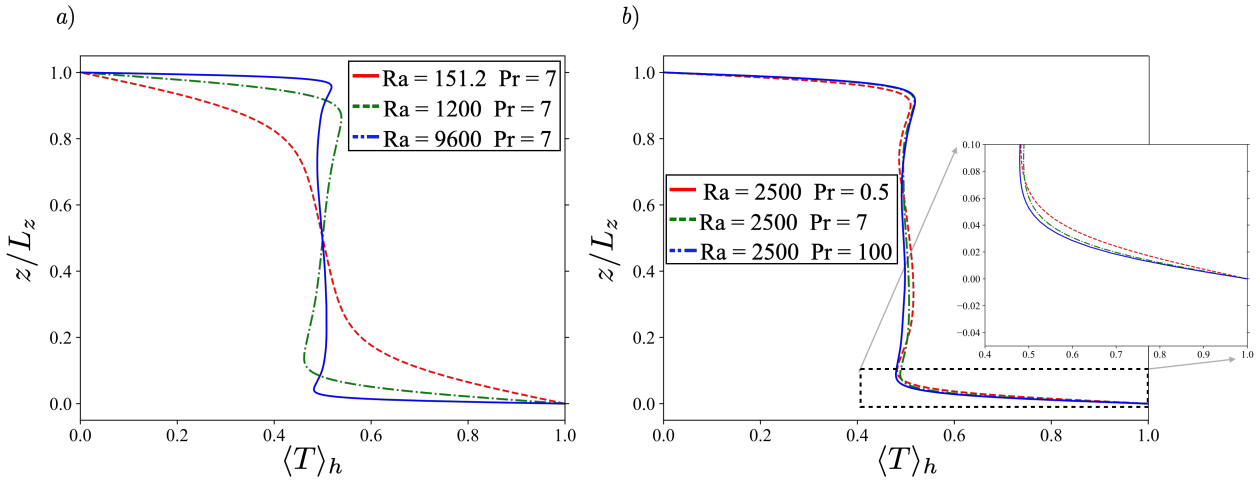

Figure 4.6: The figure presents average temperature profiles in the statistically steady state. Panel a) shows the profiles for three simulations with increasing Rayleigh numbers and the same Prandtl number, while panel b) demonstrates the impact of varying the Prandtl number while maintaining a constant Rayleigh number.

Closed-box boundary conditions (CB) were also tested, meaning no penetration in the x-direction while continuing with free slip in both the z and x directions. The aspect ratio chosen for these simulations was $L : H = 1 : 1$. In Figure 4.7, the results for these simulations are compared with the results obtained with periodic boundary conditions (PBC). It can be observed that neither the Nusselt number nor the degree of mixing of the system respond to this change in boundary conditions. This is intriguing because not only was a no-penetration restriction added but also the cell's aspect ratio was changed. This could indicate that performing simulations with an aspect ratio of $L : H = 1 : 1$ and periodic boundary conditions

would yield the same results as before, which could not only reduce the computational cost of the simulations but also be helpful to experimental physicists working with Hele-Shaw cells in the laboratory.

Furthermore, in Figure 4.7, two series for different Γ (or ϵ) values are shown. In subplot a), it can be observed that heat transport is affected by the ratio between the cell's aperture and height, decreasing as Γ increases due to the effect of corrections made to the Darcy's law. It is very interesting that the degree of mixing of the system (subplot b)) does not vary when Γ changes and follows the same behavior described in Figure 4.4. Hence, the degree of mixing does not respond to changes in the boundary conditions (from CB to PBC) or changes in Γ. Presumably, it also does not respond to variations in the Prandtl number between $[7, 100]$.

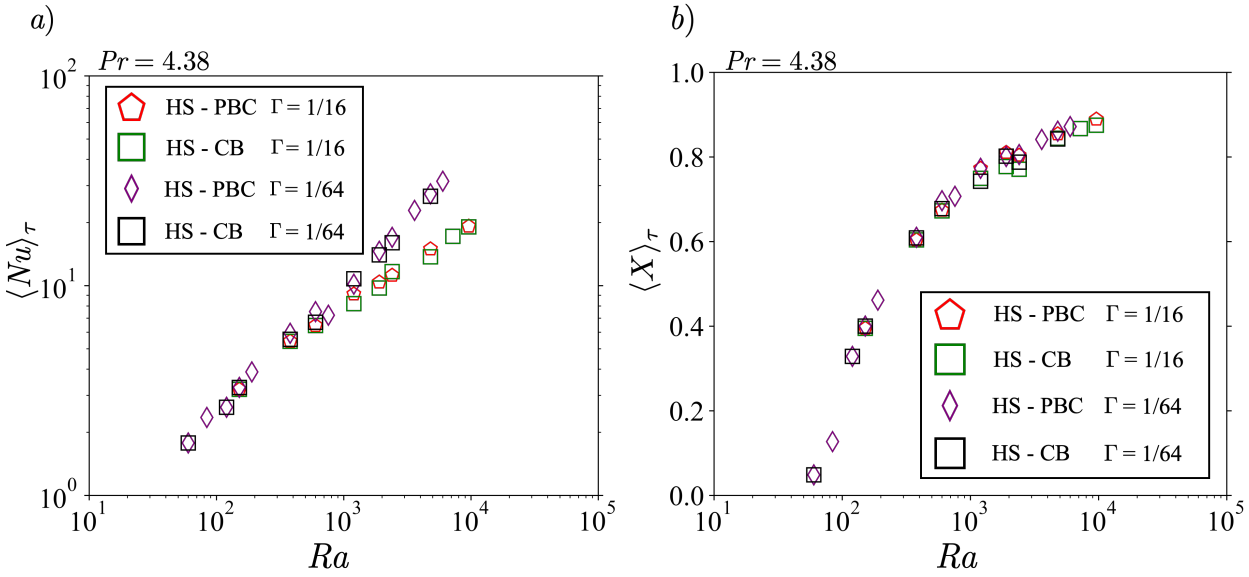

Figure 4.7: Comparison between periodic boundary conditions (PBC) and closed box boundary conditions (CB) is shown. It can be observed that both the a) Nusselt number and b) the degree of mixing are unaffected by the change in boundary conditions. Interestingly, it appears that the degree of mixing in the system does not respond to changes in Γ or ϵ.

Finally, the effect of increasing the grid size beyond the established criteria was studied. Simulations were performed that only met the criterion of having spacing smaller than the Kolmogorov scale, disregarding the Batchelor scale. In Figure 4.8, the obtained results can be seen, and it is interesting to note that for the simulation with the highest Rayleigh number, the difference, especially for the simulations with *Pr=100*, reaches up to a 25% overestimation of the heat flux. This highlights the importance of the chosen criteria and how crucial it is to adhere to them.

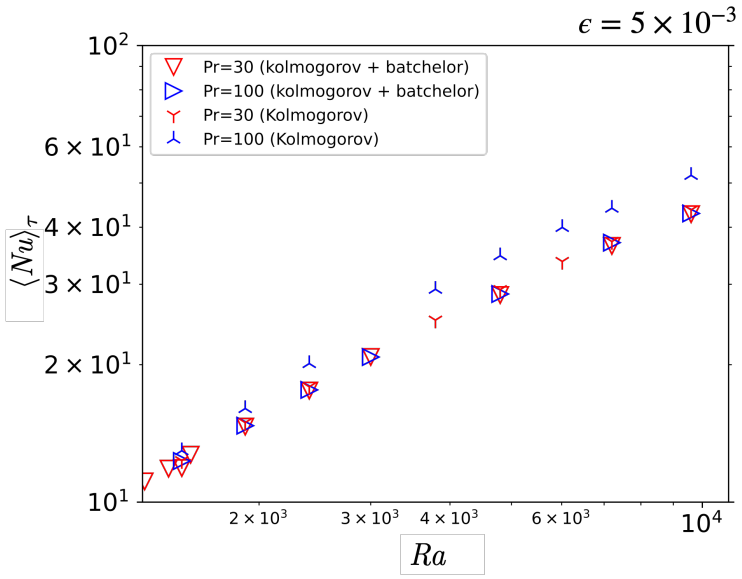

Figure 4.8: Differences between discretizations that only satisfy the criterion of being smaller than the Kolmogorov scale and those that satisfy being smaller than both the Kolmogorov scale and π times the Batchelor scale (spectral scale).

4.1.2. No Slip Simulations

One of the objectives of this work is to define the limits of the HSM accurately. For this purpose, the study conducted by Chong and Xia (2016) is a valuable reference, as it solves the motion and transport equations in 3D. However, a crucial difference exists between Chong and Xia (2016) simulations and the exploration already conducted in this study, which lies in the boundary conditions. While *flow_solve* allows the implementation of no-slip boundary conditions, it is not an easy task. Therefore, the model was implemented in *Dedalus3*, a software that allows for easy interchangeability of boundary conditions for the problem in $\hat{z}$ direction.

The first step was to perform a benchmark *flow_solve* using free-slip boundary conditions. The results are shown in Figure 4.9. Subplot a) presents a comparison between the results published in Ulloa and Letelier (2022) and the results obtained with *Dedalus3*, while subplot b) shows the comparison between the results simulated with *flow_solve* in this study and the simulations conducted with *Dedalus3*. It is evident that the implementation of the model in *Dedalus3* and the software itself work effectively, successfully reproducing the results already observed.

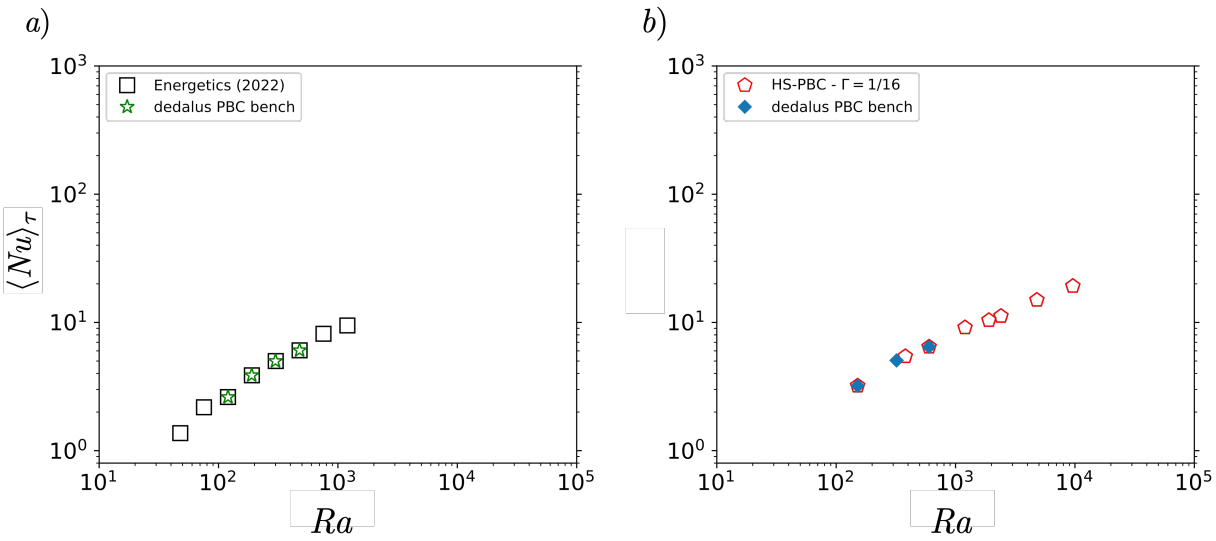

Figure 4.9: Benchmark of *Dedalus3*. a) shows the Benchmark with results obtained with *flow_solve* in Ulloa & Letelier (2022) and b) shows the benchmark with results obtained in this work with *flow_solve*.

Figure 4.10 presents the 3D simulations conducted by Chong and Xia (2016) in highly confined environments (same as in Fig 2.3), but using the Rayleigh number (Ra) commonly used in porous media. Several interesting aspects can be observed in this figure. Firstly, regardless of the confinement degree, all data collapse at the same point when the Rayleigh number approaches $4\pi^2$, which is the critical value for the onset of convection in the Darcy regime (Nield & Bejan, 2012). Secondly, for high Rayleigh values, the Nusselt numbers tend to follow the classical scaling of 3D free fluids (Ahlers et al., 2009) (this can be better observed in Fig 2.3), with a scaling law of $Nu \sim Ra^{1/3}$, which is clearly different from what happens in the Darcy model (Hewitt et al., 2012). In the Darcy regime, within this range of Rayleigh, heat is efficiently transported from wall to wall following a scaling law of $Nu \sim Ra^{0.9}$.

The truly interesting aspect for this work occurs between the onset of convection and sufficiently high Rayleigh values. In this range, the data exhibit a deviation from the results of porous media associated with weak contributions that occur in the confinement direction. Additionally, the scaling laws in these regimes are variable and depend on Γ (the cell aspect ratio). This is the Hele-Shaw regime (Letelier et al., 2019; De Paoli et al., 2020). Therefore, is it possible to reproduce these results using the set of 2D equations derived by Letelier et al. (2019)? While it is currently impossible with *Dedalus3* to impose no-slip boundary conditions on all four walls of the cell as done by Chong and Xia (2016), it is possible to impose no-slip conditions in the z-direction while maintaining periodicity in the x-direction. Due to the differences in boundary conditions, the results could also show a clear dependence of the system's response to variations in the aspect ratio L:H. These simulations serve as a first approximation to validate the model.

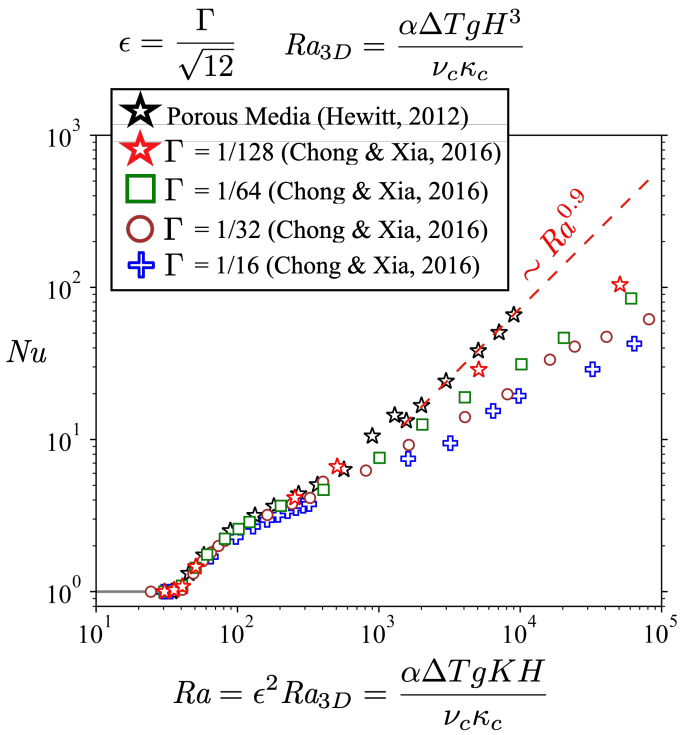

Figure 4.10: The results obtained by Chong et al. (2016) when converting 3D Rayleigh to the Rayleigh number used in porous media, Ra, for a range of $\Gamma \in [1/128, 1/16]$, are presented along with the results by Hewitt et al. (2012) for porous media convection.

Figure 4.11 presents the results obtained with *Dedalus3* using periodic boundary conditions in the x-direction and no-slip conditions in the z-direction, compared to Chong and Xia (2016) 3D closed-box simulations with no-slip conditions on all walls with $L : H = 1 : 1$. It can be observed that the *HSM* can accurately reproduce the 3D results up to an $\epsilon^2 Ra = 0.06$. However, beyond this limit, the HSM results start to deviate, overestimating the heat fluxes. Later, for a $\Gamma = 1/16$, regardless of the difference in boundary conditions, the HSM is capable of reproducing 3D results up to $\epsilon^2 Ra = 0.06$.

The discrepancy in boundary conditions is intriguing and warrants discussion. It is possible that simulating with closed-box and no-slip boundary conditions could lead to the *HSM* reproducing more values accurately. On the other hand, for low Rayleigh numbers, particularly in Darcian regimes, boundary conditions may not significantly impact the results. However, in Hele Shaw regimes, due to the increase in flow velocity, no-slip boundary conditions become increasingly important. This is also evident in Figure 4.11, where the comparison between free-slip and no-slip simulations in the z-direction is shown, as the Rayleigh increases, the greater the difference between simulations with non-slip and free slip boundary conditions. Furthermore, when comparing 3D simulations to the HSM results, it becomes evident that as the Rayleigh number increases, the disparity in Nusselt values becomes more pronounced.

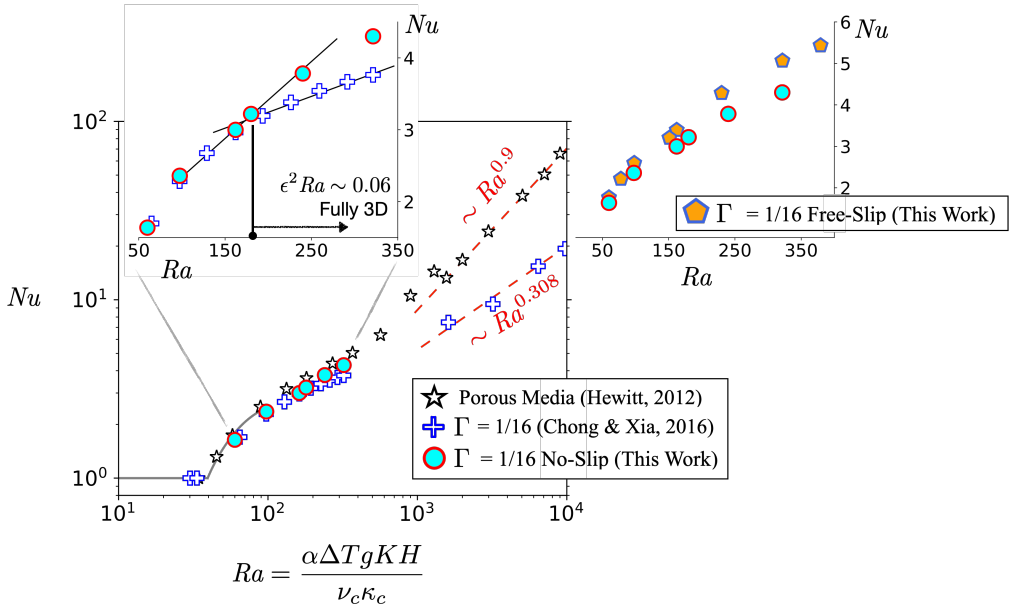

Figure 4.11: The Nusselt vs Rayleigh plot for $\Gamma = 1/16$ shows the comparison of results obtained by Chong et al. (2016) and this work, also results obtained by Hewitt (2012). In the inset plot, a departure from the data can be observed in a linear scale at $\epsilon^2 Ra = 0.06$. The graph on the right provides a comparison between simulations conducted in this study, considering both free-slip and no-slip boundary conditions. Simulations conducted using *Dedalus3*.

Figure 4.12 presents the results for $\Gamma = 1/32$ and $\Gamma = 1/64$, along with the results obtained by Chong and Xia (2016) and Hewitt et al. (2012) in the context of porous media. For low Rayleigh numbers, both our simulations in 2D (HSM) and the 3D simulations, as well as the porous media simulations, overlap. As the Rayleigh number increases, the results from the HSM and 3D simulations deviate from those of Hewitt et al. (2012), transitioning to the Hele-Shaw regime. Interestingly, it seems that the limit reached by the HSM is dependent on Γ, as it is observed that for $\Gamma = 1/32$, the limit appears to be up to $\epsilon^2 Ra = 0.1$, showing only a slight deviation as the Rayleigh number increases. This is confirmed with the case of $\Gamma = 1/64$, where it is evident that the model can faithfully reproduce the results up to $\epsilon^2 Ra = 0.1$. The computational cost of the simulations makes it difficult to further increase the Rayleigh number in both cases.

Letelier et al. (2019) found a theoretical relationship between the Nusselt number (Nu), which characterizes convective heat transfer, and the rate of destruction of thermal fluctuations, denoted as Φ_{scalar}, associated with irreversible thermal mixing ($Nu = Ra\Phi_{scalar}$) (Ulloa & Letelier, 2022). Figure 4.13 shows the behavior of $\epsilon^2 Nu/\Phi_{scalar}$ with respect to $\epsilon^2 Ra$, the fundamental quantity that determines the ability of the HSM to capture the dynamics of thermal convection in confined geometries. Remarkably, the same linear power-law relationship predicted by theory is obtained. *It is important to highlight again that the boundary conditions of the problem are not the same; Therefore, these may not be the actual limits of the Hele-Shaw mathematical model, however, they serve as a starting point for a deeper study of this model and open questions such as: Will the geometric aspect ratio L:H be important when it comes to to study the heat fluxes in these systems? Or will the point at which the*

results start to drift away from the 3D results be dependent on this geometric aspect ratio of the cell?, Are the limits dependent on Γ*? What about Prandtl?.*

Furthermore, it is crucial to emphasize the significance of the Hele-Shaw model. As seen in the previous chapter, many numerical models of geothermal reservoirs, geothermal shutdowns, or flows in porous media use the classical Darcy formulation, regardless of whether they are located in highly permeable regions, such as geological fault zones. This can lead to an overestimation of heat flows and potentially result in misguided decision-making.

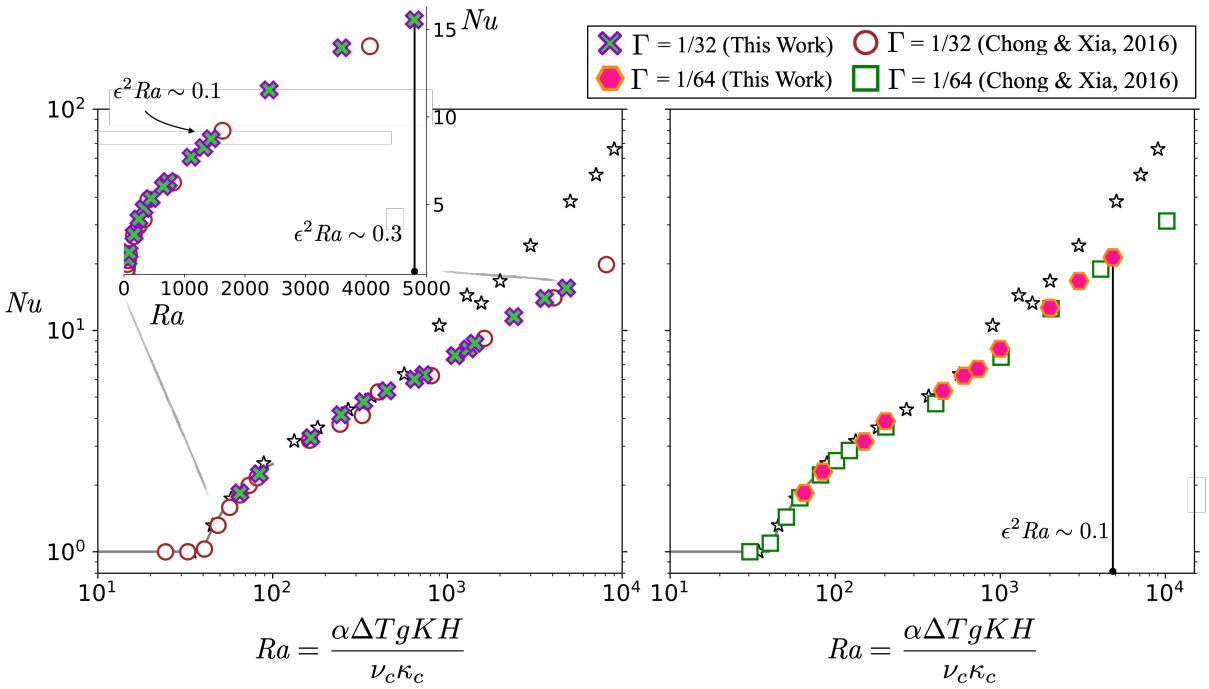

Figure 4.12: Nusselt Number versus Rayleigh Number. Panels (a) and (b) show comparative analysis of Chong 3D simulations and HSM results for $\Gamma = 1/32$ and $1/64$, respectively. Data by Hewitt, (2012) is displayed in stars. Simulations conducted using *Dedalus3*.

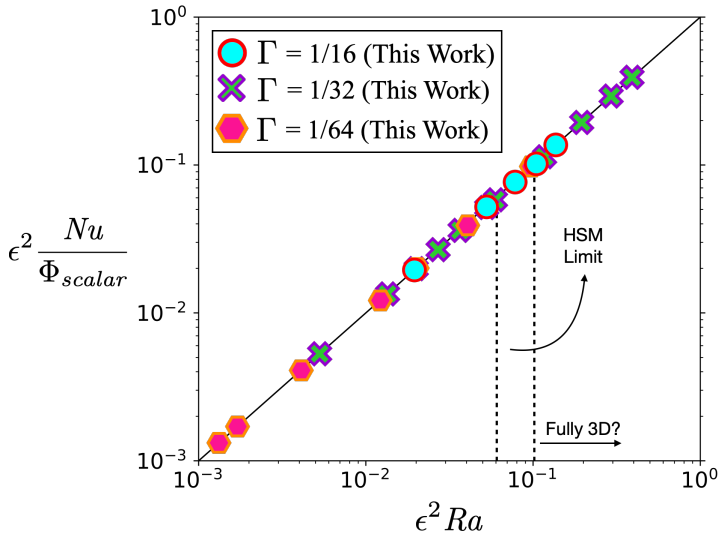

Figure 4.13: Collapsing data in a universal curve. $\epsilon^2 Nu/\Phi_{scalar}$ as a function of $\epsilon^2 Ra$.

Chapter 5

Conclusions And Future Work

5.1. Conclusions

In this section, we present a comprehensive summary of the key findings and outcomes obtained from our investigation using the Hele-Shaw model (HSM) for thermal convection in confined geometries. Through detailed numerical simulations, we have explored the behavior of heat transport and mixing dynamics under varying Rayleigh, Prandtl numbers and cell anisotropy ϵ, as well as different boundary conditions. Our study aimed to shed light on the intricate interplay between fluid flow, temperature distribution, and heat transport in confined environments, providing valuable insights for various practical applications in geothermal reservoir engineering and aquifer modeling.

The following conclusions highlight the significant observations and implications drawn from our analyses, which contribute to a deeper understanding of the thermal convection phenomena within Hele-Shaw cells or severely confined fluid environments like faults. These conclusions offer important guidance for future research directions and potential extensions of the HSM. The conclusions of this work are the following:

- With free-slip boundary conditions, in a range of $Ra \in [4\pi^2, 10000]$ and $Pr \in [7, 100]$, with $\epsilon = 0.005$, there are no major changes in heat transport varying the Prandtl number, as evidenced by the Nusselt number. The system's mixing degree behavior also shows no sensitivity to variations in Prandtl number.

- There is evidence of reduced heat transport for a simulation with a Prandtl number $Pr < 1$ specifically when $\epsilon^2 Ra/Pr \sim 0.1$. This could serve as a starting point to study the effect of inertial corrections on the system.

- For free-slip boundary conditions, the aspect ratio $L : H = 2 : 1$ with Fourier boundary conditions in $\hat{x}$ direction yields the same results as an aspect ratio of $L : H = 1 : 1$ with no-penetration boundary conditions.

- With free-slip boundary conditions, the system degree of mixing behavior appears to be minimally sensitive to changes in ϵ, at least in a range of $\epsilon \in [0.0045, 0.018]$.

- The HSM is able to reproduce a range of 3D results even with different boundary conditions in the x-direction. This may indicate that for sufficiently low Rayleigh numbers, the x-direction boundary conditions are less significant. This provides a strong step

towards validating the model. The limit in this case extends up to $\epsilon^2 Ra = 0.06$. It is emphasized that performing closed-box simulations with no-slip boundary conditions on all walls is crucial for model validation, ideally comparing with laboratory experiments as well.

- The HSM predicts a decrease in heat transport as the permeability of a medium becomes significant. This is important as many current models solely rely on the Darcy model.
- Dedalus is a valuable open-source tool that is relatively easy to use and can be instrumental in expanding the HSM's applications, such as engineering geothermal reservoirs and modeling aquifers, among others.

5.2. Future Work

The project has made significant advancements, but there are still several key tasks that remain to be completed:

- Explore inertial corrections and their accuracy: Investigate the impact of inertial corrections on the model's predictions and assess their accuracy in capturing the system's behavior accurately.
- Conduct a detailed analysis of the lower Prandtl number ($Pr < 1$) regime: Further investigate and analyze the system's dynamics in scenarios with lower Prandtl numbers to gain deeper insights into the heat transfer processes.
- Analyze cell aspect ratio effects with no-slip boundary conditions: Study the influence of different cell aspect ratios when employing no-slip boundary conditions to better understand their effects on heat transfer characteristics.
- Investigate closed box no-slip boundary conditions and their limitations: Assess the applicability and limitations of using no-slip boundary conditions in closed-box simulations and identify potential challenges.
- Study the transition between the low and high Rayleigh regime while varying Prandtl number and ϵ. Investigate how changes in these parameters influence the system's behavior during the transition, and analyze any potential trends or critical points that may arise. This investigation will provide valuable insights into the sensitivity of the model to different parameter combinations and enhance our understanding of the system's dynamics in varying regimes.
- Compare the HSM with a Forcheimer model: Perform a comparison between the Hele-Shaw model and the Forcheimer model to explore any potential links between inertial corrections and the quadratic term.
- Enhance the *Dedalus3* code: Improve the *Dedalus3* code to enable seamless integration and compatibility with the *flow_solve* files, making the analysis and simulations more convenient and user-friendly.
- Investigate the injection of a cooler fluid: Study the system's response when a cooler fluid is injected, to gain insights into heat transfer processes and potential cooling effects.

- Develop an upscaling framework for real-life applications: Work on establishing a methodology to upscale the model results for practical use in real-life scenarios, such as geothermal reservoirs.

Overall, the project has made substantial progress, and addressing these remaining tasks will lead to a comprehensive and insightful study of the Hele-Shaw model and its applicability in various scenarios.

Bibliography

Ahlers, G., Grossmann, S., & Lohse, D. (2009, 4). Heat transfer and large scale dynamics in turbulent Rayleigh-Bénard convection. *Reviews of Modern Physics*, *81*(2), 503–537. doi: 10.1103/RevModPhys.81.503

Aniss, S., Souhar, M., & Brancher, J. P. (1995). Asymptotic study and weakly nonlinear analysis at the onset of Rayleigh-Bénard convection in Hele-Shaw cell. *Physics of Fluids*, *7*(5), 926–934. doi: 10.1063/1.868568

Barbier, E. (2002). *Geothermal energy technology and current status: an overview* (Vol. 6; Tech. Rep.).

Bear, J. (1967). *A Generalized Theory on Hydrodynamic Dispersion in Porous Media* (Tech. Rep.).

Bhattacharya, S., Verma, M. K., & Samtaney, R. (2021, 6). Prandtl number dependence of the small-scale properties in turbulent Rayleigh-Bénard convection. *Physical Review Fluids*, *6*(6). doi: 10.1103/PhysRevFluids.6.063501

Bizon, C. (1997). Plume dynamics in quasi-2D turbulent convection. *Chaos*, *7*(1), 107–124. doi: 10.1063/1.166243

Blöcher, M. G., Zimmermann, G., Moeck, I., Brandt, W., Hassanzadegan, A., & Magri, F. (2010). 3D numerical modeling of hydrothermal processes during the lifetime of a deep geothermal reservoir. *Geofluids*, *10*(3), 406–421. doi: 10.1111/j.1468-8123.2010.00284.x

Bodenschatz, E., Pesch, W., & Ahlers, G. (2000). *RECENT DEVELOPMENTS IN RAYLEIGH-BÉ NARD CONVECTION* (Vol. 32; Tech. Rep.).

Bödvarsson, G. S., & Tsang, C. F. (1982, 2). Injection and Thermal Breakthrough in Fractured Geothermal Reservoirs. *Journal of Geophysical Research: Solid Earth*, *87*(B2), 1031–1048. doi: 10.1029/JB087iB02p01031

Burns, K. J., Vasil, G. M., Oishi, J. S., Lecoanet, D., & Brown, B. P. (2020, 4). Dedalus: A flexible framework for numerical simulations with spectral methods. *Physical Review Research*, *2*(2). doi: 10.1103/PhysRevResearch.2.023068

Chabora, E., Lovekin, J., Spielman, P., & Krieger, Z. (2015). *Resource Performance at Ormat's Tuscarora Geothermal Project, Nevada USA* (Tech. Rep.).

Chong, K. L., Wagner, S., Kaczorowski, M., Shishkina, O., & Xia, K. Q. (2018, 1). Effect of Prandtl number on heat transport enhancement in Rayleigh-Bénard convection under geometrical confinement. *Physical Review Fluids*, *3*(1). doi: 10.1103/PhysRevFluids.3.013501

Chong, K. L., & Xia, K. Q. (2016, 10). Exploring the severely confined regime in Rayleigh-Bénard convection. *Journal of Fluid Mechanics*, *805*, R4. doi: 10.1017/jfm.2016.578

Christensen, J. L., & Hain, D. S. (2017). Knowing where to go: The knowledge foundation for investments in renewable energy. *Energy Research and Social Science*, *25*, 124–133. doi: 10.1016/j.erss.2016.12.025

De Paoli, M., Alipour, M., & Soldati, A. (2020). How non-Darcy effects influence scaling laws in Hele-Shaw convection experiments. *Journal of Fluid Mechanics*. doi: 10.1017/jfm.2020.229

De Paoli, M., Pirozzoli, S., Zonta, F., & Soldati, A. (2022, 7). Strong Rayleigh-Darcy convection regime in three-dimensional porous media. *Journal of Fluid Mechanics*, *943*. doi: 10.1017/jfm.2022.461

Evans, D. G., & Nunn, J. A. (1989). Free thermohaline convection in sediments surrounding a salt column. *Journal of Geophysical Research*, *94*(B9). doi: 10.1029/jb094ib09p12413

Gauthier, S., Keane, C. J., Niemela, J. J., & Busse, F. H. (1978). *Reports on Progress in Physics Non-linear properties of thermal convection Non-linear properties of thermal convection* (Vol. 41; Tech. Rep.).

Grossmann, S., & Lohse, D. (2000, 3). Scaling in thermal convection: A unifying theory. *Journal of Fluid Mechanics*, *407*, 27–56. doi: 10.1017/S0022112099007545

Grossmann, S., & Lohse, D. (2001, 4). Thermal convection for large Prandtl numbers. *Physical Review Letters*, *86*(15), 3316–3319. doi: 10.1103/PhysRevLett.86.3316

Gr˜tzbach, G., & Karlsruhe, K. (1983). *Spatial Resolution Requirements for Direct Numerical Simulation of the Rayleigh-Bknard Convection* (Vol. 49; Tech. Rep.).

Hewitt, D. R. (2020, 7). Vigorous convection in porous media. *Proceedings of the Royal Society A: Mathematical, Physical and Engineering Sciences*, *476*(2239). doi: 10.1098/rspa.2020.0111

Hewitt, D. R., Neufeld, J. A., & Lister, J. R. (2012). Ultimate regime of high Rayleigh number convection in a porous medium. *Physical Review Letters*, *108*(22). doi: 10.1103/PhysRevLett.108.224503

Hewitt, D. R., Neufeld, J. A., & Lister, J. R. (2014, 5). High Rayleigh number convection in a three-dimensional porous medium. *Journal of Fluid Mechanics*, *748*(5), 879–895. doi: 10.1017/jfm.2014.216

Jonsson, T., & Catton, I. (1987). *Prandtl Number Dependence of Natural Convection in Porous Media* (Tech. Rep.).

Juncu, D., Árnadóttir, T., Geirsson, H., Guðmundsson, G. B., Lund, B., Gunnarsson, G., ... Michalczewska, K. (2020, 2). Injection-induced surface deformation and seismicity at the Hellisheidi geothermal field, Iceland. *Journal of Volcanology and Geothermal Research*, *391*. doi: 10.1016/j.jvolgeores.2018.03.019

Kamila, Z., Kaya, E., & Zarrouk, S. J. (2021). Reinjection in geothermal fields: An updated worldwide review 2020. *Geothermics*, *89*(June 2020), 101970. doi: 10.1016/j.geothermics.2020.101970

King, E. M., Stellmach, S., & Buffett, B. (2013). Scaling behaviour in Rayleigh-Bénard

convection with and without rotation. *Journal of Fluid Mechanics*, *717*, 449–471. doi: 10.1017/jfm.2012.586

Lahsen, A. (1988). Chilean geothermal resources and their possible utilization. *Geothermics*, *17*(2-3), 401–410. doi: 10.1016/0375-6505(88)90068-5

Lahsen, A., Rojas, J., Morata, D., & Aravena, D. (2015). *GEOTHERMAL EXPLORATION IN CHILE: COUNTRY UPDATE* (Tech. Rep.).

Le Reun, T., & Hewitt, D. R. (2021). High-Rayleigh-number convection in porous-fluid layers. *Journal of Fluid Mechanics*, *920*, 1–26. doi: 10.1017/jfm.2021.449

Letelier, J. A., Herrera, P., Mujica, N., & Ortega, J. H. (2016, 2). Enhancement of synthetic schlieren image resolution using total variation optical flow: application to thermal experiments in a Hele-Shaw cell. *Experiments in Fluids*, *57*(2), 1–14. doi: 10.1007/s00348-015-2109-1

Letelier, J. A., Mujica, N., & Ortega, J. H. (2019). Perturbative corrections for the scaling of heat transport in a Hele-Shaw geometry and its application to geological vertical fractures. *Journal of Fluid Mechanics*, *864*, 746–767. doi: 10.1017/jfm.2019.3

Letelier, J. A., O'Sullivan, J., Reich, M., Veloso, E., Sánchez-Alfaro, P., Aravena, D., ... Morata, D. (2021). Reservoir architecture model and heat transfer modes in the El Tatio-La Torta geothermal system, Central Andes of northern Chile. *Geothermics*, *89*(July 2020), 101940. doi: 10.1016/j.geothermics.2020.101940

Li, K., Bian, H., Liu, C., Zhang, D., & Yang, Y. (2015). Comparison of geothermal with solar and wind power generation systems. *Renewable and Sustainable Energy Reviews*, *42*, 1464–1474. doi: 10.1016/j.rser.2014.10.049

Li, T., Shiozawa, S., & McClure, M. W. (2016). Thermal breakthrough calculations to optimize design of a multiple-stage Enhanced Geothermal System. *Geothermics*, *64*, 455–465. doi: 10.1016/j.geothermics.2016.06.015

Li, X. M., He, J. D., Tian, Y., Hao, P., & Huang, S. D. (2021). Effects of Prandtl number in quasi-two-dimensional Rayleigh-Bénard convection. *Journal of Fluid Mechanics*, *915*. doi: 10.1017/jfm.2021.21

Liang, Y., Wen, B., Hesse, M. A., & DiCarlo, D. (2018, 9). Effect of Dispersion on Solutal Convection in Porous Media. *Geophysical Research Letters*, *45*(18), 9690–9698. doi: 10.1029/2018GL079849

Liu, H., Wang, H., Lei, H., Zhang, L., Bai, M., & Zhou, L. (2020). Numerical modeling of thermal breakthrough induced by geothermal production in fractured granite. *Journal of Rock Mechanics and Geotechnical Engineering*, *12*(4), 900–916. doi: 10.1016/j.jrmge.2020.01.002

Liu, S., Jiang, L., Chong, K. L., Zhu, X., Wan, Z. H., Verzicco, R., ... Sun, C. (2020). From Rayleigh-Bénard convection to porous-media convection: How porosity affects heat transfer and flow structure. *Journal of Fluid Mechanics*, *895*. doi: 10.1017/jfm.2020.309

Malkovsky, V. I., & Magri, F. (2016, 4). Thermal convection of temperature-dependent viscous fluids within three-dimensional faulted geothermal systems: Estimation from linear and numerical analyses. *Water Resources Research*, *52*(4), 2855–2867. doi: 10

.1002/2015WR018001

Malkus, W. V. R. (1954). *The Heat Transport and Spectrum of Thermal Turbulence The heat transport and spectrum of thermal turbulence** (Vol. 225; Tech. Rep. No. 1161).

Mckenzie, D. P., Roberts, J. M., & Weiss, N. . (1974). *Convection in the earth's mantle: towards a numerical simulation* (Vol. 62; Tech. Rep.).

Moeck, I. S. (2014). Catalog of geothermal play types based on geologic controls. *Renewable and Sustainable Energy Reviews*, *37*, 867–882. doi: 10.1016/j.rser.2014.05.032

Murphy, H. D. (1979). Convective instabilities in vertical fractures and faults. *Journal of Geophysical Research*, *84*(B11), 6121. doi: 10.1029/JB084iB11p06121

Murray, B. T., & Chens, C. F. (1989). *Double-diffusive convection in a porous medium* (Vol. 201; Tech. Rep.).

Nguyen, V., & Papavassiliou, D. V. (2020, 6). Hydrodynamic Dispersion in Porous Media and the Significance of Lagrangian Time and Space Scales. *Fluids*, *5*(2). doi: 10.3390/fluids5020079

Nield, D. A., & Bejan, A. (2012). *Convection in porous media: Fourth edition* (Vol. 9781461455). doi: 10.1007/978-1-4614-5541-7

Noto, D., Ulloa, H. N., & Letelier, J. A. (2023, 4). Reconstructing temperature fields for thermally-driven flows under quasi-steady state. *Experiments in Fluids*, *64*(4). doi: 10.1007/s00348-023-03620-z

Olvera-García, E., Garduño-Monroy, V. H., Ostrooumov, M., Gaspar-Patarroyo, T. L., & Nájera-Blas, S. M. (2020, 7). Structural control on hydrothermal upwelling in the Ixtlán de los Hervores geothermal area, Mexico. *Journal of Volcanology and Geothermal Research*, *399*. doi: 10.1016/j.jvolgeores.2020.106888

Otero, J., Dontcheva, L. A., Johnston, H., Worthing, R. A., Kurganov, A., Petrova, G., & Doering, C. R. (2004). High-Rayleigh-number convection in a fluid-saturated porous layer. *Journal of Fluid Mechanics*(500), 263–281. doi: 10.1017/S0022112003007298

Palm, B., Weber, O D D M U N, J. E., & Kvernvold, D. (1972). *On steady convection in a porous medium* (Vol. 54; Tech. Rep. No. 1).

Pruess, K., & Bodvarsson, G. S. (1984). Thermal Effects of Reinjection in Geothermal Reservoirs With Major Vertical Fractures. *JPT, Journal of Petroleum Technology*, *36*(10), 1567–1578. doi: 10.2118/12099-pa

Puyguiraud, A., Gouze, P., & Dentz, M. (2021, 4). Pore-Scale Mixing and the Evolution of Hydrodynamic Dispersion in Porous Media. *Physical Review Letters*, *126*(16). doi: 10.1103/PhysRevLett.126.164501

Risacher, F., Fritz, B., & Hauser, A. (2011, 2). Origin of components in Chilean thermal waters. *Journal of South American Earth Sciences*, *31*(1), 153–170. doi: 10.1016/j.jsames.2010.07.002

Saeid, S., Al-Khoury, R., & Barends, F. (2013). An efficient computational model for deep low-enthalpy geothermal systems. *Computers and Geosciences*, *51*, 400–409. doi: 10.1016/j.cageo.2012.08.019

Saffman, P. G. (1986). Viscous fingering in Hele-Shaw cells. *Journal of Fluid Mechanics*, *173*, 73–94. doi: 10.1017/S0022112086001088

Sahimi, M., & Imdakm, A. O. (1988). *The effect of morphological disorder on hydrodynamic dispersion in flow through porous media* (Vol. 21; Tech. Rep.).

Shishkina, O., Emran, M. S., Grossmann, S., & Lohse, D. (2017, 10). Scaling relations in large-Prandtl-number natural thermal convection. *Physical Review Fluids*, *2*(10). doi: 10.1103/PhysRevFluids.2.103502

Shortall, R., Davidsdottir, B., & Axelsson, G. (2015). Geothermal energy for sustainable development: A review of sustainability impacts and assessment frameworks. *Renewable and Sustainable Energy Reviews*, *44*, 391–406. doi: 10.1016/j.rser.2014.12.020

Sun, N.-Z. (1996). Hydrodynamic Dispersion in Porous Media. In *Mathematical modeling of groundwater pollution* (pp. 9–49). New York, NY: Springer New York. doi: 10.1007/978-1-4757-2558-2{_}2

Ulloa, H. N., & Letelier, J. A. (2022). Energetics and mixing of thermally driven flows in Hele-Shaw cells. *Journal of Fluid Mechanics*, *930*. doi: 10.1017/jfm.2021.897

Wang, M., & Bejan, A. (1987). *HEAT TRANSFER CORRELATION FOR BENARD CONVECTION IN A FLUID SATURATED POROUS LAYER* (Vol. 14; Tech. Rep.).

Wen, B., Chang, K. W., & Hesse, M. A. (2018). Rayleigh-Darcy convection with hydrodynamic dispersion. *Physical Review Fluids*, *3*(12), 1–18. doi: 10.1103/PhysRevFluids.3.123801

Winters, K. B., & de la Fuente, A. (2012). Modelling rotating stratified flows at laboratory-scale using spectrally-based DNS. *Ocean Modelling*, *49-50*, 47–59. doi: 10.1016/j.ocemod.2012.04.001

Yan, J., Ballmer, M. D., & Tackley, P. J. (2020, 5). The evolution and distribution of recycled oceanic crust in the Earth's mantle: Insight from geodynamic models. *Earth and Planetary Science Letters*, *537*. doi: 10.1016/j.epsl.2020.116171